The Aeronautical Journal (2025), **129**, pp. 1399–1420
doi:10.1017/aer.2024.128

ROYAL AERONAUTICAL SOCIETY

RESEARCH ARTICLE

Disturbance observer-based fixed-time tracking control for space manipulators with parametric uncertainty and unknown disturbance

Y.X. Yan[1], H. Cui[1] and P. Han[2]

[1]Deep Space Exploration Research Center, Harbin Institute of Technology, Harbin, China
[2]School of Civil Engineering, Harbin Institute of Technology, Harbin, China
Corresponding author: Y.X. Yan; Email: yanyxhit@126.com

Received: 27 February 2024; **Revised:** 16 September 2024; **Accepted:** 18 October 2024

Keywords: space manipulator; fixed-time sliding mode control; nonlinear disturbance observer; trajectory tracking

Abstract

The challenging tracking control issue for a space manipulator subject to parametric uncertainty and unknown disturbance is addressed in this paper. An observer-based fixed-time terminal sliding mode control methodology is put forward. Firstly, a nonlinear disturbance observer is introduced for exactly reconstructing the lumped uncertainty without requiring any prior knowledge of the lumped uncertainty. Meanwhile, the estimation time's upper bound is not only irrelevant to the initial estimation error but can be directly predicted in advance via a specific parameter in the observer. Invoking the estimated information, a fast fixed-time tracking controller with strong robustness is designed, where a novel sliding mode surface incorporated enables faster convergence. The globally fixed-time stability of the closed-loop tracking system is rigorously demonstrated through Lyapunov stability analysis. Finally, numerical simulations and comparisons verify the validity and superiority of the suggested controller.

Nomenclature

$\boldsymbol{r}_b$	base spacecraft position
$\boldsymbol{v}_b$	base spacecraft linear velocity
$\boldsymbol{\omega}_b$	base spacecraft angle velocity
$\boldsymbol{I}_b$	base spacecraft inertia tensor
$\boldsymbol{M}_b$	base spacecraft mass
$\boldsymbol{r}_i$	the ith link position
$\boldsymbol{v}_i$	the ith link velocity
$\boldsymbol{\omega}_i$	the ith link angle velocity
$\boldsymbol{I}_i$	the ith link inertia tensor
$\boldsymbol{M}_i$	the ith link mass
$\boldsymbol{a}_i$	position vector from the ith joint to the centre of the ith link
$\boldsymbol{b}_i$	position vector from the centre of the ith link to i+1th link
$\boldsymbol{\rho}_i$	position vector from the rigin O_I to the centre of the ith link
q_i	rotation angle of the ith joint
z_i	rotation axis of the ith joint
$\boldsymbol{r}_g$	position vector from O_I to the total centre of the system
$\boldsymbol{E}_3$	three-dimensional identity matrix
$\boldsymbol{H}$	generalised inertia matrix of space manipulator system
$\boldsymbol{C}$	Coriolis and centrifugal matrix of space manipulator system
$\boldsymbol{u}$	joint driving torque
$\boldsymbol{e}_1$	joint angle tracking error

© The Author(s), 2024. Published by Cambridge University Press on behalf of Royal Aeronautical Society.

https://doi.org/10.1017/aer.2024.128 Published online by Cambridge University Press

$\boldsymbol{e}_2$	joint velocity tracking error
$\boldsymbol{f}_{dis}$	the lumped uncertainty of the system
$\hat{\boldsymbol{f}}_{dis}$	the estimate of the lumped uncertainty of the system
$\boldsymbol{e}_f$	the disturbance observer error
T_d	the predefined observation time
$l_d, l_k, k_d, \lambda_{d1}, \lambda_{d2}, \delta_d$	positive constant
h_{1i}, h_{2i}, μ_i	positive gain
m_1, n_1, p_1, q_1	positive odd integer
k_a, k_b	positive scalars
s_n, s_r, s_m	positive constants
m_2, n_2, p_2, q_2	positive odd integer
$\gamma_1, \gamma_2, \gamma_3$	positive gain
ss_n, ss_r, ss_m	positive constant
SMS	space manupulator system
FFSM	free-floating space manipulator
DOBFTSMC	disturbance observer-based fixed-time sliding mode control
FTSMC	fixed-time sliding mode control
ANFTSMC	adaptive nonsingular fast terminal sliding mode control
D-H	Denavit-Hartenberg parameters

1.0 Introduction

Free-floating space manipulators (FFSM) have demonstrated significant potential for a variety of complicated on-orbit operations, such as constructing and maintaining space stations, removing space debris, repairing or refueling defunct satellites and so on [1–4]. One of the primary concerns in successfully accomplishing these specific space missions is precise tracking control for space manipulators. However, unlike ground-based robotic manipulators, any movement of the manipulator can interfere with the translation and rotation of the base spacecraft, and vice versa. Notably, the high non-linearity and strong coupling characteristics of the dynamic model present tremendous challenges to the trajectory-tacking process of FFSM. What's worse, it is inherently vulnerable to unknown disturbance and parametric uncertainty in complex space environment, which deteriorates tracking performance even further. Consequently, designing an advanced tracking control system with strong robustness and high reliability is essential for FFSM.

Only the asymptotic convergence is guaranteed despite the fact that numerous control strategies are accessible for space manipulators, including adaptive technique [5], backstepping technique [6], neural network technique [7], model predictive technique [8, 9], sliding mode control (SMC) [10, 11] and H_∞ control [12]. Nonetheless, from a practical perspective, rapid and flexible manoeuvering of manipulators plays a crucial role in the execution of aerospace activities. Finite-time control, as opposed to the asymptotic control, provides quick convergence of the state variables within a confined time while enhancing control accuracy. Terminal SMC was presented in Ref. [13] as a dependable method for finite-time control of a space rigid manipulator. Nevertheless, when the system state value approaches zero, terminal SMC encounters a singularity issue. To resolve the issue, a non-singular terminal sliding mode control (NTSMC) was designed for FFSM vulnerable to external disturbance [14]. A neural network adaptive NTSMC-based finite-time formation tracking controller was designed for a space manipulator under actuator saturation [15]. To tolerate different undesirable actuator faults, a continuous tracking control strategy based on integral sliding surface was also devised for a space manipulator in Ref. [16]. By utilising the homogeneous technique, a reliable robust controller was designed for an uncertain space manipulator to enable finite-time trajectory tracking [17]. Nevertheless, there is an obvious disadvantage to these finite-time control schemes: the required settling time is extremely sensitive to the system's initial conditions.

To overcome such weakness, a fixed-time stability control strategy was developed, which can guarantee that the convergence time is confined by a positive constant [18]. The significant characteristic of this

https://doi.org/10.1017/aer.2024.128 Published online by Cambridge University Press

methodology is that the control coefficient is the sole determinant of the settling time. Owing to such an outstanding attribute, control schemes based on the fixed-time stabilisation concept have attracted a lot of attention recently. Through a combination of fixed-time control and extended state observer, a robust task-space trajectory tracking control strategy was presented for a space manipulator with model uncertainties and unknown velocities [19]. With the help of the backstepping technique, a fault-tolerant control approach was proposed for a free-flying space manipulator, which enables fixed-time trajectory tracking while satisfying output constraints [20]. Besides, fixed-time control is frequently applied in conjunction with SMC. Cao et al. [21] extended the conventional fixed-time stability system and proposed a faster terminal SMC for the attitude stabilisation of rigid spacecraft. To deal with the singularity issue, a piecewise fast terminal sliding surface was developed in Ref. [22] to ensure that the system state was practical fixed-time stable. Liu et al. [23] proposed a general class of non-singular predefined-time SMC mechanism, which was implemented in the tracking control of a two-arm space manipulator. In Ref. [24], a non-singular fault-tolerant trajectory tracking control strategy based on a fast fixed-time stable system was designed for unmanned surface vehicles. Nonetheless, the current fixed-time SMC schemes do not have a rapid enough convergence rate, especially when the system state is close to the equilibrium point. As a result, there is still an open topic for developing a faster fixed-time SMC controller.

A potential problem in the application of fixed-time SMC is the requirement of the disturbance's upper bound, which is hard to determine in practice. To deal with this issue, several disturbance rejection techniques including the adaptive method [25], the time-delay estimation method [26, 27] and the observer-based method [28, 29] are typically introduced to attenuate the negative effects of disturbance. Among them, the disturbance observer-based control techniques have attracted considerable attention because of straightforward structure and excellent estimation performance. An observer-based two scale robust control strategy was presented for space manipulators to eliminate the effects of external disturbance [30]. In Ref. [31], an adaptive sliding mode disturbance observer was presented for estimating and compensating the model uncertainty of space manipulators. Even though the system uncertainty's derivative has an unknown bound, it is still achievable for the finite-time disturbance estimation. Recently, a robust fixed-time tracking control scheme was investigated for FFSM, where the system's total uncertainties can be accurately and quickly estimated by designing a disturbance observer [32]. It should be noted that the majority of the existing disturbance observers were developed based on the assumption of either known disturbance upper bounds or limited disturbance time derivatives. Such restrictive assumptions let the controllers hold certain conservative, and thus the issue of releasing such constraints is required to be further explored.

Inspired by the above-mentioned considerations, this work investigates a unique observer-based fast fixed-time SMC tracking strategy for FFSM suffering from parametric uncertainty and unknown disturbance. The primary contributions of this research are concisely summarised in the following:

- A novel fast and singularity-free stable system is put forward to assure theoretical global fixed-time convergence. In comparison to the existing fixed-time stable systems in Refs [33, 34], the suggested stable system exhibits a faster convergence.
- A nonlinear disturbance observer is built to facilitate quick and precise disturbance estimation while requiring no prior information about the lumped uncertainty. Moreover, a distinctive feature of the suggested observer is that the estimation error is stable within a specific time that can be arbitrarily determined in advance because it is explicitly expressed in the observer.
- Based on the reconstructed uncertainties, a unique faster sliding mode tracking controller is devised, which guarantees the position and velocity tracking errors converge to zero within a given time even in the case of lumped uncertainty. The suggested approach has greater application potential due to the advantages in convergence speed and control precision.

The remainder of this work is structured as follows. Section 2 gives the system modelling and formulates the problem. Section 3 presents the main result. Section 4 illustrates numerical simulations and comprehensive comparisons. Section 5 draws conclusion.

https://doi.org/10.1017/aer.2024.128 Published online by Cambridge University Press

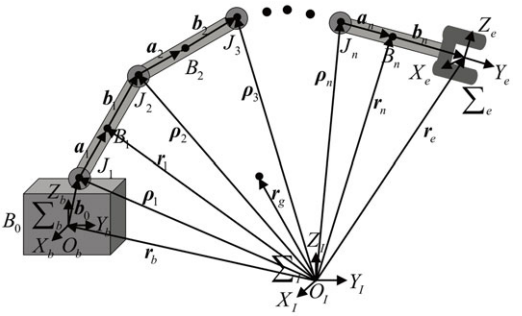


Figure 1. *System model for a free-floating space manipulator.*

2.0 System description and problem statement

2.1 Notations and lemmas

Notations. $\mathbf{z} = [z_1, z_2, \ldots, z_n]^{\mathrm{T}}$ is an n-dimensional vector with the ith element z_i. The symbols $\| \cdot \|$ denotes the Euclidean norm of a vector or the induced norm of a matrix. For a positive constant $a > 0$, define the vector $\mathrm{sig}^a(\mathbf{z}) = \left[|z_1|^a \mathrm{sign}\,(z_1)\,, |\,z_2|^a \mathrm{sign}\,(z_2)\,, \ldots, |z_n|^a \mathrm{sign}\,(z_n)\right]^{\mathrm{T}}$ and the vector $\mathrm{sgn}(\mathbf{z}) = [\mathrm{sign}\,(z_1)\,, \mathrm{sign}\,(z_2)\,, \ldots, \mathrm{sign}\,(z_n)\,]^{\mathrm{T}}$.

Definition 1. ([35]) *Consider a nonlinear system*

$$\dot{\boldsymbol{y}}(t) = g\,(\boldsymbol{y}(t))\,, \boldsymbol{y}\,(\boldsymbol{0}) = \boldsymbol{y}_0, \boldsymbol{y} \in \mathbb{R}^n \tag{1}$$

If the system (1) is finite-time convergent and the settling time $t\,(\boldsymbol{y}_0)$ *is bounded for all initial states, then the system's equilibrium is said to be fixed-time stable, i.e.,* $\exists t_{max} > 0$ *such that* $t\,(y_0) \leq t_{max}, \forall \boldsymbol{y}_0 \in \mathbb{R}^n$.

Lemma 1. ([36, 37]) *Let* $v_j \geq 0\ (j = 1, 2, \ldots, N)$*, for two constants* w_1 *and* w_2 *satisfying* $0 < w_1 \leq 1$ *and* $w_2 > 1$*, the following inequalities hold*

$$\sum_{j=1}^{N} v_j^{w_1} \geq \left(\sum_{j=1}^{N} v_j\right)^{w_1}, \sum_{j=1}^{N} v_j^{w_2} \geq N^{1-w_2}\left(\sum_{j=1}^{N} v_j\right)^{w_2} \tag{2}$$

2.2 Mathematical modelling

For the final approaching phase of target capture, the primary objective is to precisely manoeuver the joint in accordance with the planned trajectory. To describe the space manipulator 's trajectory tracking issue, the reference coordinate systems, which include the inertial coordinate system $O_I X_I Y_I Z_I$ and the body coordinate system $O_b X_b Y_b Z_b$, are depicted in Fig. 1. In the free-floating mode, the spacecraft has its control system turned off and there is no external force or torques acting on the system. Therefore, motion of the manipulator will result in translation and rotation of the spacecraft. Considering the actual working environment of FFSM, the following reasonable assumptions are given [14]:

Assumption 1. *Since FFSM works in the microgravity environment, the effects of gravity are ignored during modeling. Besides, all parts of the system are rigid, and the flexibility influences and the solar panels are neglected.*

Assumption 2. *All the links of FFSM are connected by revolute joints and have an open chain kinematic configuration. Since the system work in free-floating mode, the spacecraft can rotate around three axes and move in three directions.*

Assumption 3. *In the case of free-floating, the system satisfies the condition of momentum conservation. In other words, the system's linear and angular momentum are both constant.*

https://doi.org/10.1017/aer.2024.128 Published online by Cambridge University Press

Based on the relative relations in Fig. 1, the position vector from B_i to O_I can be represented as:

$$\boldsymbol{r}_i = \boldsymbol{r}_b + \boldsymbol{b}_0 + \sum_{j=1}^{i-1} \left(\boldsymbol{a}_j + \boldsymbol{b}_j\right) + \boldsymbol{a}_i \quad i = 1, 2, \ldots, n \tag{3}$$

The line and angular velocity of B_i can be expressed as

$$\boldsymbol{v}_i = \boldsymbol{v}_b + \boldsymbol{\omega}_b \times (\boldsymbol{r}_i - \boldsymbol{r}_b) + \sum_{j=1}^{i} \left(z_j \times \left(\boldsymbol{r}_i - \boldsymbol{\rho}_j\right)\right) \dot{q}_j \tag{4}$$

$$\boldsymbol{\omega}_i = \boldsymbol{\omega}_b + \sum_{j=1}^{i} \dot{q}_j \boldsymbol{z}_j \tag{5}$$

For zero initial momentum, the conservation equation of an FFSM system can be deduced as

$$\begin{bmatrix} \boldsymbol{P} \\ \boldsymbol{L} \end{bmatrix} = \begin{bmatrix} M_g \boldsymbol{E}_3 & M_g \left(\boldsymbol{r}_{bg}^{\times}\right)^T \\ M_g \boldsymbol{r}_{bg}^{\times} & \boldsymbol{H}_{\omega} \end{bmatrix} \begin{bmatrix} \boldsymbol{v}_b \\ \omega_b \end{bmatrix} + \begin{bmatrix} \boldsymbol{J}_{T\omega} \\ \boldsymbol{H}_{\omega\phi} \end{bmatrix} \dot{\boldsymbol{q}} = \boldsymbol{0} \tag{6}$$

where the system total linear momentum $\boldsymbol{P} = M_b \boldsymbol{v}_b + \sum_{i=1}^{n} M_i \boldsymbol{v}_i$, and the system total angular momentum $\boldsymbol{L} = I_b \boldsymbol{\omega}_b + \boldsymbol{r}_b \times M_b \boldsymbol{v}_b + \sum_{i=1}^{n} \boldsymbol{I}_i \omega_i + \sum_{i=1}^{n} (r_i \times \boldsymbol{M}_i \boldsymbol{r}_i)$, the total mass $M_g = M_b + \sum_{i=1}^{n} M_i$, $\boldsymbol{r}_{bg} = \boldsymbol{r}_g - \boldsymbol{r}_b$, $\boldsymbol{H}_{\omega} = \sum_{i=1}^{n} \left(\boldsymbol{I}_i - M_i (\boldsymbol{r}_i - \boldsymbol{r}_b)^{\times} (\boldsymbol{r}_i - \boldsymbol{r}_b)^{\times}\right) + \boldsymbol{I}_b$, $\boldsymbol{H}_{\omega\phi} = \sum_{i=1}^{n} (\boldsymbol{I}_i \boldsymbol{J}_{\omega i} + M_i (\boldsymbol{r}_i - \boldsymbol{r}_b) \times \boldsymbol{J}_{Ti})$, $\boldsymbol{J}_{T\omega} = \sum_{i=1}^{n} (M_i \boldsymbol{J}_{Ti})$, $\boldsymbol{J}_{\omega i} = \begin{bmatrix} z_1 & z_2 & \ldots & \boldsymbol{0}_{3\times(n-i)} \end{bmatrix}$, and $\boldsymbol{J}_{Ti} = \begin{bmatrix} \mathbf{z}_1 \times (\mathbf{r}_i - \rho_1) \ldots \mathbf{z}_i \times (\mathbf{r}_i - \rho_i) \, \boldsymbol{0}_{3\times(n-i)} \end{bmatrix}$. Moreover, the total kinetic energy of the FFSM can be derived

$$T = \frac{1}{2} \left(\boldsymbol{\omega}_b^T I_b \omega_b + M_b \boldsymbol{v}_b^T \boldsymbol{v}_b + \sum_{i=1}^{n} \left(\omega_i^T I_i \omega_i + M_i \boldsymbol{v}_i^T \boldsymbol{v}_i\right) \right) \tag{7}$$

Substituting (4)–(6) into (7) and rearranging it, ones eventually have

$$T = \frac{1}{2} \dot{\boldsymbol{q}}^{\mathrm{T}} \boldsymbol{H} \dot{\boldsymbol{q}} \tag{8}$$

where $\boldsymbol{H}$ is called the generalised inertia tensor of the space manipulator, which can expressed as $\boldsymbol{H} = \boldsymbol{H}_m + \boldsymbol{H}_{bm}^{\mathrm{T}} \boldsymbol{J}_{bm}$. And the matrices $\boldsymbol{H}_m$ is the inertia matrix of the manipulator, $\boldsymbol{J}_{bm}$ is the Jacobian matrix between the base spacecraft and the manipulator, and $\boldsymbol{H}_{bm}$ is the coupling matrix between the base spacecraft and the manipulator.

Considering the time-varying disturbances, the mathematical model of FFSM through the application of the Lagrange equation is given by:

$$\boldsymbol{H}(\boldsymbol{q})\ddot{\boldsymbol{q}} + \boldsymbol{C}(\boldsymbol{q}, \dot{\boldsymbol{q}})\dot{\boldsymbol{q}} = \boldsymbol{u} + \boldsymbol{d}(t) \tag{9}$$

where, $\boldsymbol{q}$, $\dot{\boldsymbol{q}}$, $\ddot{\boldsymbol{q}} \in \mathbb{R}^n$ are the joint generalised position, velocity and acceleration vectors, respectively. The inertia matrix $\boldsymbol{H}(\boldsymbol{q}) \in \mathbb{R}^{n\times n}$ is described by $\boldsymbol{H}(\boldsymbol{q}) = \boldsymbol{H}_0(\boldsymbol{q}) + \boldsymbol{\Delta} H(\boldsymbol{q})$, and the Coriolis and Centrifugal matrix $\boldsymbol{C}(\boldsymbol{q}, \dot{\boldsymbol{q}}) \in \mathbb{R}^{n\times n}$ is described by $\boldsymbol{C}(\boldsymbol{q}, \dot{\boldsymbol{q}}) = \boldsymbol{C}_0(\boldsymbol{q}, \dot{\boldsymbol{q}}) + \Delta \boldsymbol{C}(\boldsymbol{q}, \dot{\boldsymbol{q}})$, in which $\boldsymbol{H}_0(\boldsymbol{q})$ and $\boldsymbol{C}_0(\boldsymbol{q}, \dot{\boldsymbol{q}})$ indicate the nominal matrices, $\Delta \boldsymbol{H}(\boldsymbol{q})$ and $\Delta \boldsymbol{C}(\boldsymbol{q}, \dot{\boldsymbol{q}})$ represent the deviations caused by the parametric uncertainty, $\boldsymbol{d}(t) \in \mathbb{R}^n$ denotes the time-varying disturbance acting on the space manipulator system, and $\boldsymbol{u} \in \mathbb{R}^n$ represents the control input.

Considering the desired position and velocity $\boldsymbol{q}_d$ and $\dot{\boldsymbol{q}}_d$, define $\boldsymbol{e}_1 = \boldsymbol{q}_1 - \boldsymbol{q}_d$ and $\boldsymbol{e}_2 = \dot{\boldsymbol{q}}_1 - \dot{\boldsymbol{q}}_d$ as position and velocity tracking errors, respectively. The system (9) can be then rewritten as

$$\begin{cases} \dot{\boldsymbol{e}}_1 = \boldsymbol{e}_2 \\ \dot{\boldsymbol{e}}_2 = \boldsymbol{H}_0^{-1}(\boldsymbol{q})\boldsymbol{u} - \boldsymbol{H}_0^{-1}(\boldsymbol{q})\boldsymbol{C}_0(\boldsymbol{q}, \dot{\boldsymbol{q}})\dot{\boldsymbol{q}} + \boldsymbol{f}_{dis} - \ddot{\boldsymbol{q}}_d \end{cases} \tag{10}$$

where $\boldsymbol{f}_{dis}$ is lumped uncertainty denoted by $\boldsymbol{f}_{dis} = \boldsymbol{H}_0^{-1}(\boldsymbol{q}) \left(\boldsymbol{d} - \Delta \boldsymbol{H}(\boldsymbol{q})\ddot{\boldsymbol{q}} - \Delta \boldsymbol{C}(\boldsymbol{q}, \dot{\boldsymbol{q}})\dot{\boldsymbol{q}}\right)$.

https://doi.org/10.1017/aer.2024.128 Published online by Cambridge University Press

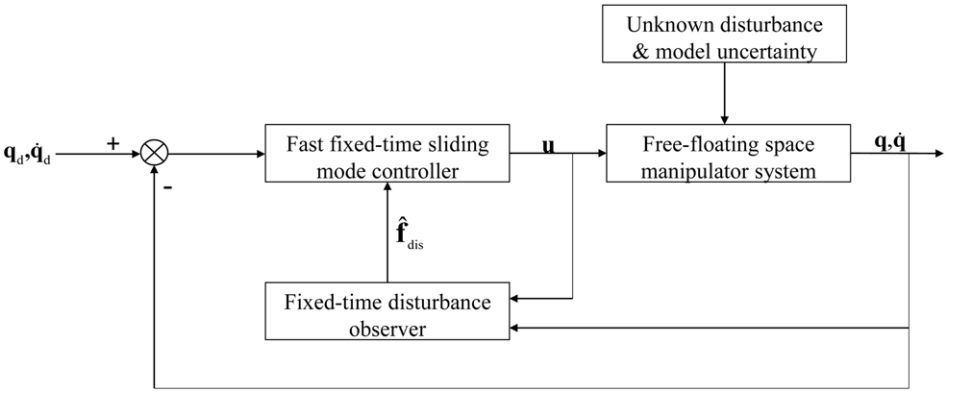


Figure 2. *The structure diagram of the closed-loop tracking system.*

Assumption 4. *Given bounded inertial uncertainty and unknown disturbance, the lumped uncertainty* $\boldsymbol{f}_{dis}$ *is assumed to be bounded, which satisfies* $\left\|\boldsymbol{f}_{dis}\right\| \leq d_m$ *with an unknown constant* $d_m > 0$.

2.3 Problem description

The primary objective for a joint-space task typically requires the FFSM to precisely track the desired joint trajectory. In this context, the tracking issue can be described as: despite the unknown disturbance and parametric uncertainty, for any initial states design a tracking controller $\boldsymbol{u}$ for FFSM system such that the desired trajectory $\boldsymbol{q}_d$ is followed within a fixed time, i.e., the tracking errors $\boldsymbol{e}_1$ and $\boldsymbol{e}_2$ are fixed-time stable.

3.0 Main results

This section presents the research's primary outcomes. First, a new fast fixed-time stability system is developed which enables faster convergence. For determining the lumped uncertainty estimation, a nonlinear disturbance observer is subsequently constructed. Finally, a robust fixed-time sliding mode tracking controller is designed employing the reconstructed uncertainty information. Figure 2 depicts the schematic structure for the suggested closed-loop tracking system.

3.1 A novel fast fixed-time stability system

Theorem 1. *When a system satisfies*

$$\dot{x} = -N(x)\left(c_1 sig^{1+\sigma_0}(x) + c_2 sig^{\lambda_0}(x)\right) \tag{11}$$

where $\sigma_0 = \frac{m_0}{2n_0}(1 + sgn(|x|-1)) + \left(\frac{p_0}{2q_0} - \frac{1}{2}\right)(1 - sgn(|x|-1))$, $\lambda_0 = \left(\frac{p_0}{q_0} + \frac{m_0}{2n_0}\right) + \left(1 - \frac{p_0}{q_0} + \frac{m_0}{2n_0}\right) sgn(|x|-1)$, $c_1 > 0$ *and* $c_2 > 0$ *are two scalars,* $m_0 > 0$, $n_0 > 0$, $p_0 > 0$, *and* $q_0 > 0$ *are odd integers, which satisfy* $m_0 > n_0$ *and* $\frac{q_0}{2} < p_0 < q_0$. $N(x) = 1 + 2_a arctan\left(s_b |x|^{s_c}\right)/\pi$ *with* $s_a > 0$, $s_b > 0$ *and* $s_c > 0$ *satisfying* $s_c = \begin{cases} s_c & |x| \geq 1 \\ 1 & |x| < 1 \end{cases}$. *Then the system (11) is fixed-time stable and the convergence time* T_c *is bounded by*

$$T_c \leq \frac{q_0}{(q_0 - p_0)c_1}\left(1 - \frac{c_2}{c_1}\ln\left(1 + \frac{c_1}{c_2}\right)\right) + \frac{n_0}{(c_1 + c_2)m_0} \tag{12}$$

https://doi.org/10.1017/aer.2024.128 Published online by Cambridge University Press

Proof. Introduce a variable $\Psi = |x|^{1-\frac{p_0}{q_0}}$ and its time derivative can be obtained

$$\begin{aligned}\dot{\Psi} &= \left(1-\frac{p_0}{q_0}\right)\mathrm{sig}^{-\frac{p_0}{q_0}}(x)\,\dot{x}\\ &= -\left(1-\frac{p_0}{q_0}\right)N(x)\left(c_1\left|x\right|^{1+\sigma_0-\frac{p_0}{q_0}}+c_2\left|x\right|^{\lambda_0-\frac{p_0}{q_0}}\right)\\ &= -\left(1-\frac{p_0}{q_0}\right)N(x)\left(c_1|\Psi|^{\varepsilon}+c_2|\Psi|^{\gamma}\right)\end{aligned} \tag{13}$$

where $\varepsilon = 1+\frac{\sigma_0 q_0}{q_0-p_0}$ and $\gamma = \frac{\lambda_0 q_0-p_0}{q_0-p_0}$.

According the definitions of σ_0 and λ_0, it can be known that

$$\begin{cases}\varepsilon=\gamma=1+\dfrac{m_0 q_0}{n_0(q_0-p_0)} & |x|\geq 1\\ \varepsilon=0,\ \gamma=-1 & |x|<1\end{cases} \tag{14}$$

Solving (13), the convergence time is derived

$$\begin{aligned}T_c &= \frac{q_0}{q_0-p_0}\int_0^{\Psi(0)}\frac{d\Psi}{N(x)\left(c_1|\Psi|^{\varepsilon}+c_2|\Psi|^{\gamma}\right)}\\ &= \frac{q_0}{q_0-p_0}\left(\int_0^1\frac{d\Psi}{N(x)\left(c_1|\Psi|^{\varepsilon}+c_2|\Psi|^{\gamma}\right)}+\int_1^{\Psi(0)}\frac{d\Psi}{N(x)\left(c_1|\Psi|^{\varepsilon}+c_2|\Psi|^{\gamma}\right)}\right)\\ &= \frac{q_0}{q_0-p_0}\left(\int_0^1\frac{d\Psi}{N(x)\left(c_1+c_2|\Psi|^{-1}\right)}+\int_1^{\Psi(0)}\frac{d\Psi}{N(x)\left(c_1+c_2\right)|\Psi|^{\rho}}\right)\end{aligned} \tag{15}$$

where $\rho = 1+\frac{m_0 q_0}{n_0(q_0-p_0)}$.

Since $1\leq N(x)<1+s_a$, then one has

$$\begin{aligned}T_c &\leq \frac{q_0}{q_0-p_0}\left(\int_0^1\frac{d\Psi}{c_1+c_2|\Psi|^{-1}}+\int_1^{\Psi(0)}\frac{d\Psi}{(c_1+c_2)|\Psi|^{\rho}}\right)\\ &\leq \frac{q_0}{q_0-p_0}\left\{\frac{1}{c_1}\left(1-\frac{c_2}{c_1}\ln\left(1+\frac{c_1}{c_2}\right)\right)+\frac{1-\Psi(0)^{1-\rho}}{(c_1+c_2)(\rho-1)}\right\}\end{aligned} \tag{16}$$

Invoking $\rho = 1+\frac{m_0 q_0}{n_0(q_0-p_0)}>1$ and $\Psi(0)>0$, the settling time T_c is given by

$$T_c \leq \frac{q_0}{(q_0-p_0)c_1}\left(1-\frac{c_2}{c_1}\ln\left(1+\frac{c_1}{c_2}\right)\right)+\frac{n_0}{(c_1+c_2)m_0} \tag{17}$$

□

Remark 1. As shown in (17), the upper bound of the convergence time T_c depends only on the system parameters $p_0, q_0, m_0, n_0, c_1, c_2$ regardless of any system initial states.

Remark 2. Zuo et al. [33] constructed a fixed-time stable system (named FTSS1) $\dot{x} = -c_1 x^{m_0/n_0}-c_2 x^{p_0/q_0}$. Ni et al. [38] investigated a fast fixed-time stable system (called FTSS2) $\dot{x} = -c_1 x^{\frac{1}{2}+\frac{m_0}{2n_0}+\left(\frac{m_0}{2n_0}-\frac{1}{2}\right)sgn(|x|-1)}-c_2 x^{p_0/q_0}$. By observation, the convergence time of FTSS1 and FTSS2 can be uniformly calculated as

$$T_F = \frac{q_0}{q_0-p_0}\left(\int_0^1\frac{1}{c_1 W+c_2}dW+\int_1^{W(0)}\frac{1}{c_1 W^{\zeta}+c_2}dW\right) \tag{18}$$

where $\zeta = 1$ for FTSS1 and $\zeta = 1+\frac{(m_0-n_0)q_0}{n_0(q_0-p_0)}$ for FTSS2. Due to the fact the inequality $\frac{1}{c_1 W+c_2}>\frac{1}{c_1+c_2 W^{-1}}$ holds for $W\in(0,1)$, and the inequality $\frac{1}{c_1 W^{\zeta}+c_2}>\frac{1}{(c_1+c_2)W^{\rho}}$ holds for $W\in(1,+\infty)$, it is concluded that the proposed fixed-time stable system (11) attains a faster convergence rate than FTSS1 and FTSS2.

https://doi.org/10.1017/aer.2024.128 Published online by Cambridge University Press

3.2 Nonlinear disturbance observer design

The system (10) can be represented as

$$\dot{\boldsymbol{e}}_2 = -l_d \boldsymbol{e}_2 + \boldsymbol{H}_0^{-1}(\boldsymbol{q})\boldsymbol{u} + \boldsymbol{F}_d \tag{19}$$

where l_d is a positive gain, and $\boldsymbol{F}_d = -\boldsymbol{H}_0^{-1}(\boldsymbol{q})\boldsymbol{C}_0(\boldsymbol{q}, \dot{\boldsymbol{q}})\dot{\boldsymbol{q}} + \boldsymbol{f}_{dis} - \ddot{\boldsymbol{q}}_d + l_d \boldsymbol{e}_2$.

For system (19), introduce an auxiliary system as

$$\dot{z}_d = -l_d z_d + \boldsymbol{H}_0^{-1}(\boldsymbol{q})\boldsymbol{u} \tag{20}$$

where $z_d \in \mathbb{R}^{n\times n}$ is the state of the auxiliary system.

Define x_d as the deviation between e_2 and $\mathbf{z}_d$, which is expressed as $x_d = e_2 - z_d$. Then, the time derivative of x_d yields

$$\dot{x}_d = -l_d x_d + F_d \tag{21}$$

Theorem 2. *Construct a nonlinear disturbance observer as*

$$\begin{aligned}\dot{\hat{\boldsymbol{x}}}_d = &-l_k k_d \hat{\boldsymbol{x}}_d + l_k^{-1}\dot{\boldsymbol{y}}_d + k_d \boldsymbol{y}_d \\ &+ \frac{n^{\frac{\delta_d}{4}}\pi}{2\delta_d T_d \sqrt{\lambda_{d1}\lambda_{d2}}}\left(\lambda_{d1} sig^{1+\delta_d}(\boldsymbol{e}_d) + \lambda_{d2} sig^{1-\delta_d}(\boldsymbol{e}_d)\right)\end{aligned} \tag{22}$$

with its output provided by

$$\hat{\boldsymbol{f}}_{dis} = \hat{\boldsymbol{F}}_d + \boldsymbol{H}_0^{-1}(\boldsymbol{q})\boldsymbol{C}_0(\boldsymbol{q}, \dot{\boldsymbol{q}})\dot{\boldsymbol{q}} + \ddot{\boldsymbol{q}}_d - l_d \boldsymbol{e}_2 \tag{23}$$

with

$$\hat{\boldsymbol{F}}_d = l_k^{-1}\boldsymbol{y}_d + l_d \hat{\boldsymbol{x}}_d \tag{24}$$

where $\hat{\boldsymbol{x}}_d$ and $\hat{\boldsymbol{f}}_{dis}$ denote the estimations of $\boldsymbol{x}_d$ and $\boldsymbol{f}_{dis}$, respectively. $\boldsymbol{y}_d = l_k \boldsymbol{x}_d$, $l_k > 0$, $k_d > 0$, $0 < \delta_d < 1$, λ_{d1} and λ_{d2} are two positive constants, T_d is an adjustable parameter that characterises the convergence time. Then, the observer error $\boldsymbol{e}_d = \boldsymbol{x}_d - \hat{\boldsymbol{x}}_d$ and the disturbance estimation error $\boldsymbol{e}_f = \boldsymbol{f}_{dis} - \hat{\boldsymbol{f}}_{dis}$ are fixed-time stable, and the convergence time T_e is bounded by T_d.

Proof. The observer error dynamics can be given by

$$\begin{aligned}\dot{\boldsymbol{e}}_d &= \dot{\boldsymbol{x}}_d - \dot{\hat{\boldsymbol{x}}}_d \\ &= \dot{\boldsymbol{x}}_d + l_k k_d \hat{\boldsymbol{x}}_d - l_k^{-1}\dot{\boldsymbol{y}}_d - k_d \boldsymbol{y}_d \\ &\quad - \frac{n^{\frac{\delta_d}{4}}\pi}{2\delta_d T_d \sqrt{\lambda_{d1}\lambda_{d2}}}\left(\lambda_{d1} sig^{1+\delta_d}(\boldsymbol{e}_d) + \lambda_{d2} sig^{1-\delta_d}(\boldsymbol{e}_d)\right) \\ &= -l_k k_d \boldsymbol{e}_d - \frac{n^{\frac{\delta_d}{4}}\pi}{2\delta_d T_d \sqrt{\lambda_{d1}\lambda_{d2}}}\left(\lambda_{d1} sig^{1+\delta_d}(\boldsymbol{e}_d) + \lambda_{d2} sig^{1-\delta_d}(\boldsymbol{e}_d)\right)\end{aligned} \tag{25}$$

Choose a Lyapunov function as $V_d = e_d^{\mathrm{T}} e_d$, and its time derivation can be obtained

$$\begin{aligned}\dot{V}_d &= 2e_d^T \dot{\boldsymbol{e}}_d \\ &= -2l_k k_d e_d^T e_d - \frac{n^{\frac{\delta_d}{4}}\pi}{\delta_d T_d \sqrt{\lambda_{d1}\lambda_{d2}}}\left(\sum_{i=1}^{n}\lambda_{d1}|e_{di}|^{2+\delta_d} + \sum_{i=1}^{n}\lambda_{d2}|e_{di}|^{2-\delta_d}\right)\end{aligned} \tag{26}$$

According to Lemma 1, $\dot{V}_d$ has the following inequality relation

$$\dot{V}_d \le -\frac{n^{\frac{\delta_d}{4}}\pi}{\delta_d T_d \sqrt{\lambda_{d1}\lambda_{d2}}}\left\{n^{-\frac{\delta_d}{2}}\lambda_{d1} V_d^{\delta_d} + \lambda_{d2}\right\} V_d^{\frac{2-\delta_d}{2}} \tag{27}$$

https://doi.org/10.1017/aer.2024.128 Published online by Cambridge University Press

Define $\chi_d = n^{-\frac{\delta_d}{4}}\sqrt{\frac{\lambda_{d1}}{\lambda_{d2}}}V_d^{\frac{\delta_d}{2}}$, then $d\chi_d = \frac{\delta_d}{2}n^{-\frac{\delta_d}{4}}\sqrt{\frac{\lambda_{d1}}{\lambda_{d2}}}V_d^{\frac{\delta_d}{2}-1}dV_d$. Then, solving the inequality (27) yields $V_d(t) \equiv 0$ for $t \geq T_e$, and T_e is bounded by

$$\begin{aligned} T_e &\leq \frac{\delta_d T_d \sqrt{\lambda_{d1}\lambda_{d2}}}{n^{\frac{\delta_d}{4}}\pi}\int_0^{V_d(0)} \frac{V_d^{\frac{\delta_d}{2}-1}}{\left\{n^{-\frac{\delta_d}{2}}\lambda_{d1}V_d^{\delta_d}+\lambda_{d2}\right\}}dV_d \\ &\leq \frac{2T_d}{\pi}\int_0^{\chi_d(0)} \frac{d\chi_d}{\left\{\chi_d^2+1\right\}} \\ &\leq \frac{2T_d}{\pi}\arctan\left(\chi_d\left(0\right)\right) \end{aligned} \tag{28}$$

Since $0 < arctan\left(\chi_d\left(0\right)\right) < \frac{\pi}{2}$, one has

$$T_e \leq T_d \tag{29}$$

Consequently, it is shown that the observer error e_d is fixed-time stable. Applying (23), the disturbance estimation error $\boldsymbol{e}_f$ is derived

$$\begin{aligned} \boldsymbol{e}_f &= \boldsymbol{f}_{dis} - \hat{\boldsymbol{f}}_{dis} \\ &= \boldsymbol{F}_d + \boldsymbol{H}_0^{-1}(\boldsymbol{q})\boldsymbol{C}_0(\boldsymbol{q},\dot{\boldsymbol{q}})\dot{\boldsymbol{q}} + \ddot{\boldsymbol{q}}_d - l_d\boldsymbol{e}_2 \\ &\quad - \hat{\boldsymbol{F}}_d - \boldsymbol{H}_0^{-1}(\boldsymbol{q})\boldsymbol{C}_0(\boldsymbol{q},\dot{\boldsymbol{q}})\dot{\boldsymbol{q}} - \ddot{\boldsymbol{q}}_d + l_d\boldsymbol{e}_2 \\ &= \boldsymbol{F}_d - \hat{\boldsymbol{F}}_d \end{aligned} \tag{30}$$

From (21), it follows $\boldsymbol{F}_d = \dot{\boldsymbol{x}}_d + l_d\boldsymbol{x}_d$. Applying (24), Equation (30) can be simplified as

$$\begin{aligned} \boldsymbol{e}_f &= \dot{\boldsymbol{x}}_d + l_d\boldsymbol{x}_d - l_k^{-1}\dot{\boldsymbol{y}}_d - l_d\hat{\boldsymbol{x}}_d \\ &= l_d\boldsymbol{e}_d \end{aligned} \tag{31}$$

As a result, it can be conclude that $\boldsymbol{e}_f = \boldsymbol{0}$ is obtained for $t \geq T_e$. This means that the lumped uncertainty $\boldsymbol{f}_{dis}$ can be reconstructed by $\hat{\boldsymbol{f}}_{dis}$ after the specific time T_d. □

Remark 3. The primary highlights of the suggested disturbance observer (22) are as follows:

1. Contrary to the existing observers in Refs [19, 31, 39, 40], there is a relaxation of restrictive assumptions that the lumped disturbance and corresponding time-derivative have to be bounded or know. The suggested disturbance observer (22) requires no prior knowledge of the lumped disturbance, which allows for a wider rage of applications.
2. Even when the initial estimation error tends to infinity, the precise estimate of lumped uncertainty is guaranteed within a finite time. Unlike most existing fixed-time observers, the settling time is explicitly specified through an individual parameter T_d in the proposed observer without the requirement for tedious parameter adjustment.

3.3 Tracking controller design and stability analysis

Based on Theorem 1, a novel non-singular fixed-time terminal sliding mode surface (NFTSMS) is presented as

$$\boldsymbol{s} = \boldsymbol{e}_2 + N(\boldsymbol{e}_1)\left(k_a\boldsymbol{S}_c + k_b\boldsymbol{S}_z\right) \tag{32}$$

where $k_a > 0$ and $k_b > 0$ are two scalars, $N\left(\boldsymbol{e}_1\right) = 1 + 2s_m\arctan\left(s_n e_1^{s_r}\right)/\pi$ with $s_n > 0$, $s_m > 0$ and $s_r > 0$ satisfying $s_r = \begin{cases} s_r & ||\boldsymbol{e}_1|| \geq 1 \\ 1 & ||\boldsymbol{e}_1|| < 1 \end{cases}$. S_{ci} and S_{zi} are respectively the ith elements of $\boldsymbol{S}_c$ and $\boldsymbol{S}_z$, and have the following forms

https://doi.org/10.1017/aer.2024.128 Published online by Cambridge University Press

$$S_{ci}=\begin{cases}\text{sig}^{1+2\sigma_1}(e_{1i}) & \text{if} \quad \bar{s}_i=0 \text{ or } \overline{s_i}\neq 0, |\mathrm{e}_{1i}|\geq\delta\\ l_1e_{1i}+l_2e_{1i}^2\text{sgn}(e_{1i})+l_3e_{1i}^3 & \text{if} \quad \bar{s}_i\neq 0, |\mathrm{e}_{1i}|<\delta\end{cases}$$

$$S_{zi}=\begin{cases}\text{sig}^{2\lambda_1-1}(\mathrm{e}_{1i}) & \text{if} \quad \overline{s_i}=0 \quad \text{or} \quad \overline{s_i}\neq 0, |\mathrm{e}_{1i}|\geq\delta\\ g_1e_{1i}+g_2e_{1i}^2\,\text{sgn}(e_{1i})+g_3e_{1i}^3 & \text{if} \quad \overline{s_i}\neq 0, |\mathrm{e}_{1i}|<\delta\end{cases} \tag{33}$$

where $i=1,2,\ldots,n$, $\sigma_1=\frac{m_1}{2n_1}(1+\text{sgn}(||\boldsymbol{e}_1||-1))+\left(\frac{p_1}{2q_1}-\frac{1}{2}\right)(1-\text{sgn}(||\boldsymbol{e}_1||-1))$, $\lambda_1=\left(\frac{p_1}{q_1}+\frac{m_1}{2n_1}\right)+\left(1-\frac{p_1}{q_1}+\frac{m_1}{2n_1}\right)\text{sgn}(||\boldsymbol{e}_1||-1)$ with $m_1>n_1$ and $\frac{3}{4}q_1<p_1<q_1$, $0<\delta<1$ is a constant. To make the functions S_{ci} and S_{zi}, and their time derivative continuous, the values of l_1, l_2, l_3, g_1, g_2, g_3 are chosen as [41]

$$\begin{aligned}
l_1&=(2p_1/q_1-3)(p_1/q_1-2)\,\delta^{2p_1/q_1-2}\\
l_2&=-(2p_1/q_1-2)(2p_1/q_1-4)\,\delta^{2p_1/q_1-3}\\
l_3&=(p_1/q_1-1)(2p_1/q_1-3)\,\delta^{2p_1/q_1-4}\\
g_1&=(4p_1/q_1-5)(2p_1/q_1-3)\,\delta^{4p_1/q_1-4}\\
g_2&=-(4p_1/q_1-4)(4p_1/q_1-6)\,\delta^{4p_1/q_1-5}\\
g_3&=(2p_1/q_1-2)(4p_1/q_1-5)\,\delta^{4p_1/q_1-6}\\
\bar{\boldsymbol{s}}&=\boldsymbol{e}_2+N(\boldsymbol{e}_1)\left(k_a sig^{1+2\sigma_1}(\boldsymbol{e}_1)+k_b sig^{2\lambda_1-1}(\boldsymbol{e}_1)\right)
\end{aligned} \tag{34}$$

Let $\boldsymbol{G}(\boldsymbol{e}_1)=N(\boldsymbol{e}_1)(k_a\boldsymbol{S}_c+k_b\boldsymbol{S}_z)$. And taking the time derivative of the NFTSMS by using (10) yields

$$\begin{aligned}
\dot{\boldsymbol{s}}&=\dot{\boldsymbol{e}}_2+\dot{\boldsymbol{G}}\\
&=\boldsymbol{H}_0^{-1}(\boldsymbol{q})\boldsymbol{u}-\boldsymbol{H}_0^{-1}(\boldsymbol{q})\boldsymbol{C}_0(\boldsymbol{q},\dot{\boldsymbol{q}})\dot{\boldsymbol{q}}+\boldsymbol{f}_{dis}-\ddot{\boldsymbol{q}}_d+\dot{\boldsymbol{G}}
\end{aligned} \tag{35}$$

To obtain accurate and fast trajectory tracking, design an observer-based fixed-time SMC strategy as

$$\boldsymbol{u}=\boldsymbol{u}_1+\boldsymbol{u}_2 \tag{36}$$

where

$$\boldsymbol{u}_1=-\boldsymbol{H}_0(\boldsymbol{q})\hat{\boldsymbol{f}}_{dis}+\boldsymbol{C}_0(\boldsymbol{q},\dot{\boldsymbol{q}})\dot{\boldsymbol{q}}+\boldsymbol{H}_0(\boldsymbol{q})\ddot{\boldsymbol{q}}_d-\boldsymbol{H}_0\dot{\boldsymbol{G}} \tag{37}$$

$$\boldsymbol{u}_2=-\boldsymbol{H}_0(\boldsymbol{q})N(\boldsymbol{s})\left(\gamma_1\text{sig}^{1+2\sigma_2}(\boldsymbol{s})+\gamma_2\text{sig}^{2\lambda_2-1}(\boldsymbol{s})+\gamma_3\boldsymbol{s}\right) \tag{38}$$

where $\sigma_2=\frac{m_2}{2n_2}(1+\text{sgn}(\|s\|-1))+\left(\frac{p_2}{2q_2}-\frac{1}{2}\right)(1-\text{sgn}(\|s\|-1))$, $\lambda_2=\left(\frac{p_2}{q_2}+\frac{\sigma_2}{2}\right)+\left(1-\frac{p_2}{q_2}+\frac{\sigma_2}{2}\right)\text{sgn}(\|s\|-1)$ with $m_2>n_2$ and $\frac{q_2}{2}<p_2<q_2$. $\gamma_1,\gamma_2,\gamma_3$ are positive control gains, $N(s)=1+2ss_m\arctan(ss_n\|s\|^{ss_r})/\pi$ with $ss_m>0$, $ss_n>0$ and $ss_m>0$ satisfying $ss_r=\begin{cases}ss_r & ||\boldsymbol{s}||>1\\ 1 & ||\boldsymbol{s}||<1\end{cases}$.

Theorem 3. *Considering the space manipulator system (10), once the nonlinear disturbance observer (22)–(23) reconstructs the lumped uncertainty, then the fixed-time tracking controller (36)–(38) with the NFTSMS (32) guarantees the closed-loop system is fixed-time stable.*

Proof. Substituting the controller (36) into (35) yields

$$\boldsymbol{s}=-N(\boldsymbol{s})\left(\gamma_1\text{sig}^{1+2\sigma_2}(\boldsymbol{s})+\gamma_2\text{sig}^{2\lambda_2-1}(\boldsymbol{s})+\gamma_3\boldsymbol{s}\right)-\hat{\boldsymbol{f}}_{dis}+\boldsymbol{f}_{dis} \tag{39}$$

https://doi.org/10.1017/aer.2024.128 Published online by Cambridge University Press

Choose a Lyapunov function as $V_1 = \frac{1}{2}\boldsymbol{s}^{\mathrm{T}}\boldsymbol{s}$, and one obtains

$$\begin{aligned}\dot{V}_1 &= \boldsymbol{s}^{\mathrm{T}}\dot{\boldsymbol{s}} \\ &= -N(\boldsymbol{s})\left(\gamma_1 \parallel \mathrm{s}\parallel^{2+2\sigma_2} + \gamma_2 \parallel \boldsymbol{s}\parallel^{2\lambda_2} + \gamma_3 \parallel \boldsymbol{s}\parallel^2\right) + \boldsymbol{s}^{\mathrm{T}}\boldsymbol{e}_f \\ &\le -N(\boldsymbol{s})\gamma_1 2^{1+\sigma_2}\left(\frac{1}{2}\boldsymbol{s}^{\mathrm{T}}\boldsymbol{s}\right)^{1+\sigma_2} - N(\boldsymbol{s})\gamma_2 2^{\lambda_2}\left(\frac{1}{2}\boldsymbol{s}^{\mathrm{T}}\boldsymbol{s}\right)^{\lambda_2} + \boldsymbol{s}^{\mathrm{T}}\boldsymbol{e}_f\end{aligned} \tag{40}$$

Since $\boldsymbol{e}_f = 0$ is obtained for $t \ge T_d$, the above inequality is simplified as

$$\dot{V}_1 \le -N(\boldsymbol{s})\left(\rho_1 V_1^{1+\sigma_2} - \rho_2 V_1^{\lambda_2}\right) \tag{41}$$

where $\rho_1 = \gamma_1 2^{1+\sigma_2}$, $\rho_2 = \gamma_2 2^{\lambda_2}$.

Similar to the analysis and demonstration of Theorem 1, the sliding surface NFTSMS is fixed-time stable. Noted that the sliding surface converges to the origin only if it is guaranteed that both the observation system and the sliding surface converge. Taking this into account, the convergence time t_r satisfies $t_r \ge \max\{T_d, T_r\}$, where $T_r \le \frac{n_2}{(\rho_1+\rho_2)m_2} + \frac{q_2}{(q_2-p_2)\rho_1}\left(1 - \frac{\rho_2}{\rho_1}\ln\left(1+\frac{\rho_1}{\rho_2}\right)\right)$. As a result, the system states are capable of reaching the sliding surface under the proposed controller after fixed-time t_r.

Once the system states reach the NFTSMS, i.e., $\boldsymbol{s} = \boldsymbol{0}$, the ideal sliding motion satisfies the following differential equation

$$\begin{aligned}\boldsymbol{e}_2 &= -N(\boldsymbol{e}_1)\left(k_a\boldsymbol{S}_c + k_b\boldsymbol{S}_z\right) \\ &= -N(\boldsymbol{e}_1)\left(k_a\mathrm{sig}^{1+2\sigma_1}(\boldsymbol{e}_1) + k_b\mathrm{sig}^{2\lambda_1-1}(\boldsymbol{e}_1)\right)\end{aligned} \tag{42}$$

Choose a Lyapunov function candidate $V_2 = e_1^{\mathrm{T}}e_1$, its time derivative yields

$$\begin{aligned}\dot{V}_2 &= -2N(\boldsymbol{e}_1)\boldsymbol{e}_1^T\left(k_a\mathrm{sig}^{1+2\sigma_1}(\boldsymbol{e}_1) + k_b\mathrm{sig}^{2\lambda_1-1}(\boldsymbol{e}_1)\right) \\ &= -2N(\boldsymbol{e}_1)\left(k_a V_1^{1+\sigma_1} + k_b V_1^{\lambda_1}\right)\end{aligned} \tag{43}$$

Invoking Theorem 1, the tracking errors $\boldsymbol{e}_1$ and $\boldsymbol{e}_2$ are proved to converge to the origin along the proposed NFTSMS (32) within a fixed-time t_s, which is given by

$$t_s \le \frac{n_1}{2\left(k_a + k_b\right)m_1} + \frac{q_1}{2\left(q_1 - p_1\right)k_a}\left(1 - \frac{k_b}{k_a}\ln\left(1 + \frac{k_a}{k_b}\right)\right) \tag{44}$$

Through the above demonstrations, it is concluded that the system states are fixed-time stable with the convergence time T_s satisfying $T_s \le t_r + t_s$. □

Remark 4. Noted that $\dot{\boldsymbol{y}}_d$ and $\dot{\boldsymbol{G}}$ are respectively contained in the disturbance observer (22) and the control law $\boldsymbol{u}_1$ (37), which are required to adopt the presented methodology. To satisfy this requirement, an exact fixed-time estimation of the input signal's derivatives is obtained by utilising the following uniform robust exact differentiator (URED) [42]

$$\begin{aligned}\dot{\hat{\xi}}_{1i} &= -h_{1i}\left(\mathrm{sig}^{\frac{1}{2}}\left(\hat{\xi}_{1i} - v_i\right) + \mu_i\mathrm{sig}^{\frac{3}{2}}\left(\hat{\xi}_{1i} - v_i\right)\right) + \hat{\xi}_{2i} \\ \dot{\hat{\xi}}_{2i} &= -h_{2i}\left(\frac{1}{2}\mathrm{sign}\left(\hat{\xi}_{1i} - v_i\right) + 2\mu_i\left(\hat{\xi}_{1i} - v_i\right) + \frac{3}{2}\mu_i^2\mathrm{sig}^2\left(\hat{\xi}_{1i} - v_i\right)\right)\end{aligned} \tag{45}$$

where $i = 1, 2, \ldots, n$, ξ_{1i} and ξ_{2i} are the estimations of input v_i and its derivative $\dot{v}_i$, respectively, h_{1i}, h_{2i} and μ_i are positive gains. According to Ref. [42], the differentiator (45) enables to guarantee that the states $\hat{\xi}_{1i}$ and $\hat{\xi}_{2i}$ converge to v_i and its derivative within a fixed time with respect to the parameters h_{1i}, h_{2i} and μ_i.

https://doi.org/10.1017/aer.2024.128 Published online by Cambridge University Press

Table 1. *Physical parameters of the studied space manipulator*

Parameter		B_0	B_1	B_2	B_3	B_4	B_5	B_6	B_7
mass (kg)		100	4.25	7	7	4.25	4.25	4.25	4.25
b_i (m)		0.6	0.3	0.25	0.25	-0.25	0.25	0.25	0.3
		0	0	0	0	0	0	0	0
		0	0	0.25	0.25	0	0	0	0
a_i (m)		0	0.3	0.25	0.25	-0.25	0.25	0.25	0.3
		0	0	0	0	0	0	0	0
		0	0	0.25	0.25	0	0	0	0
I_i $(\mathrm{kg}\cdot\mathrm{m}^2)$	I_{xx}	2000	0.05	0.09	0.09	0.05	0.05	0.05	1.28
	I_{yy}	2000	1.28	1.46	1.46	0.89	0.89	0.89	1.28
	I_{zz}	2000	1.28	1.46	1.46	0.89	0.89	0.89	0.05
	I_{xy}	0	0	0	0	0	0	0	0
	I_{xz}	0	0	0	0	0	0	0	0
	I_{yz}	0	0	0	0	0	0	0	0

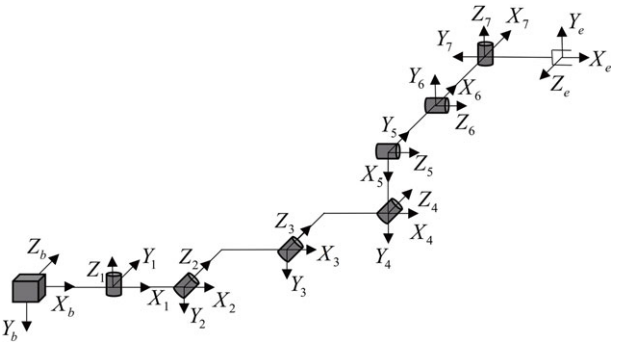


Figure 3. *D-H model of the studied space manipulator system.*

4.0 Simulation results

To demonstrate the suggested disturbance observer-based fixed-time sliding mode control (denoted DOBFTSMC) framework, numerical simulations are performed on a 7 Dof space manipulator system, whose detail physical parameters and D-H model are shown in Table 1 and Fig. 3, respectively. Noted that this paper ignores the joint trajectory planning issue, and focuses on the joint-space operations of FFSM in the presence of uncertainty. Without loss of generality, the system's initial conditions and joint desired trajectories are set the same as those in Ref. [43]. Taking into consideration model uncertainty, the nominal mass of every component in the system is assumed to be 0.9 times its actual mass. The system's time-varying disturbances are provided by $\boldsymbol{d}(t) = [d_1, d_2, d_3, d_4, d_5, d_6, d_7]^{\mathrm{T}}\mathrm{Nm}$ with $d_1 = 0.03\sin(t)$, $d_2 = 0.03\sin(2t)$, $d_3 = 0.01\sin(t)$, $d_4 = 0.01\sin(2t)$, $d_5 = 0.02\sin(t)$, $d_6 = 0.01\sin(3t)$, and $d_7 = 0.02\sin(3t)$.

The numerical simulations can be separated into three following sections. In the first section, the effectiveness of the proposed observer (22) is illustrated in terms of fixed-time convergence as well as convergence time tunability. In the second section, the superiority of the proposed DOBFTSMC is confirmed through a comparison with two other existing fixed-time control schemes. In the third section, the robustness of the proposed DOBFTSMC is demonstrated against parameter uncertainty and time-varying disturbance through Monte Carlo tests.

https://doi.org/10.1017/aer.2024.128 Published online by Cambridge University Press

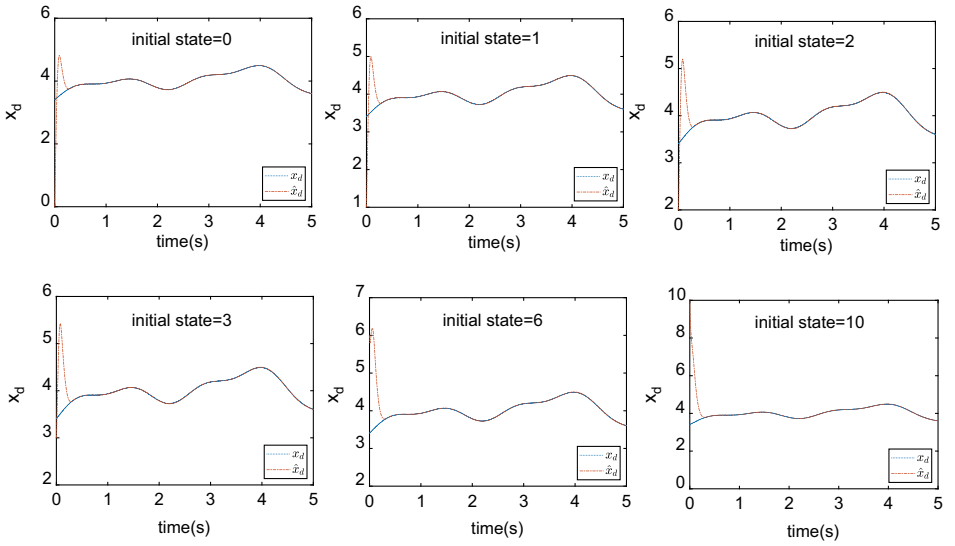


Figure 4. *Observer output for the reference signal with different initial states.*

4.1 Verification of the suggested disturbance observer

This section primarily aims to demonstrate the estimation performance of the suggested observer (22). Considering various complex disturbances that may be in the space environment, the reference signal $x_d = 3 + \sin(0.5t) + 0.3\sin(2t) + 0.2\cos(0.1t) + 0.1\sin(5t) + 0.2e^{-t} + 0.01\text{rand}(1)$ is simulated, and no reconstruction of the lumped disturbance is involved here, which will be discussed in Section 4.2. The simulation results are verified from the following two scenarios.

The proposed observer's fixed-time convergence characteristic is evaluated in the first scenario. This simulation tests six possibilities with various initial states. The observer gains are selected as $k_d = 0.1, l_d = 2, T_d = 1, \delta_d = 0.2, \lambda_{d1} = 4, \lambda_{d2} = 3, h_1 = 10, h_2 = 50, \mu = 2$. The observer's output for the reference signal is illustrated in Fig. 4. As illustrated, it is apparent that the settling time of the observer consistently remains approximately the same, regardless of the distinct values chosen for the initial conditions. In addition, the actual convergence time is observed to be significantly less than the predetermined time T_d which is attributed to the fact that T_d represents the upper bound of the convergence time. This implies that, regardless of the initial conditions, the precise estimate is always achieved within the predefined time. This fixed-time convergence feature provides increased flexibility and predictability in the observation phase.

In the second scenario, the convergence time tunability of the suggested observer is assessed via selecting multiple predetermined settling times for an identical beginning state. The observer gains are the same as the first scenario expect that T_d is different. For a given initial state value of 2, the simulation chooses T_d to be 0.5, 1.5, 3, 5, 8 and 10 seconds, respectively. Figure 5 manifests the observer's output for the reference signal under various predefined times. The observation process for the reference signal adjusts in conjunction with T_d changes. More detailed, the larger T_d is, the more time it takes to accurately estimate the reference signal. Additionally, it can be concluded from Fig. 5, that the observer can realise the precise estimation of the reference signal within the predefined time T_d. The predefined time allows straightforward and simplistic adjustment in (22), which is the intention of the observer proposed in the present research.

4.2 Verification of the suggested fixed-time tracking controller

This section focuses on the effectiveness of the proposed DOBFTSMC strategy against parametric uncertainty and time-varying disturbance. Table 2 lists the selected control parameters. The simulation

https://doi.org/10.1017/aer.2024.128 Published online by Cambridge University Press

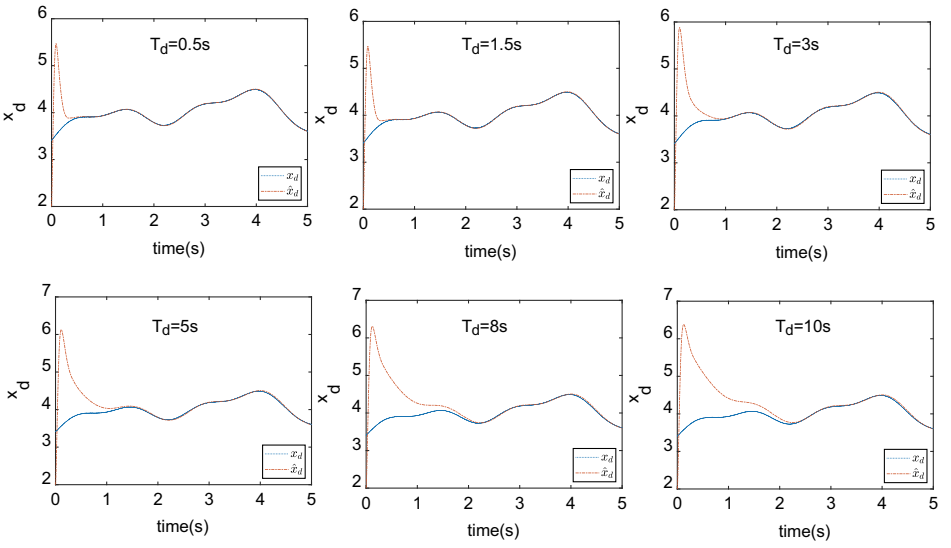


Figure 5. *Observer output for the reference signal with different predefined times.*

results ensured by the suggested approach are displayed in Figs 6 and 7. The analysis in Section 3 is well-verified by those results. As depicted in Figs 6(a) and (b), the space manipulator under the suggested control strategy can accomplish the trajectory tracking manoeuver after a brief amount of time (approximately 1.2 seconds), even in the presence of uncertain parameter and time-varying disturbance. Figure 6(c) depicts the sliding surface's time response. With the application of the proposed control law, the sliding surface is fixed-time stable, which is consistent with Theorem 3. The requested control torque is shown in Figs 6(d). Figure 7 gives the estimation performance of lumped disturbance under the proposed controller. As shown, the lumped disturbance can be precisely estimated in an extremely short period of time. This indicates that the suggested disturbance observer may accurately observe and quickly reconstruct the lumped disturbance within a predetermined time though the information of disturbance is unknown. Based on the feed-forward compensation of the constructed disturbance observer, the suggested controller achieves outstanding disturbance attenuation and satisfying tracking performance, simultaneously.

To further highlight the superiority of the suggested fixed-time control strategy, comparisons are carried out with fixed-time terminal sliding mode control (FTSMC) in Ref. [33] and adaptive nonsingular fast terminal sliding mode control (ANFTSMC) in Ref. [34]. The corresponding controllers for space manipulator can be formulated as follows:

The FTSMC is written as

$$\begin{aligned}
\boldsymbol{u} &= \boldsymbol{u}_1 + \boldsymbol{u}_2 \\
\boldsymbol{u}_1 &= \boldsymbol{C}_0(\boldsymbol{q}, \dot{\boldsymbol{q}})\dot{\boldsymbol{q}} + \boldsymbol{H}_0(\boldsymbol{q})\ddot{\boldsymbol{q}}_d - \boldsymbol{H}_0(\boldsymbol{q})\zeta \,\mathrm{sgn}(\boldsymbol{s}) \\
&\quad - \boldsymbol{H}_0(\boldsymbol{q})\boldsymbol{\sigma}^{-1}\boldsymbol{\Phi}\boldsymbol{e}_2 - \frac{p_1}{q_1}\boldsymbol{H}_0(\boldsymbol{q})\boldsymbol{\sigma}^{-1}\mathrm{diag}\left(|\sigma_i e_{2i}|^{1-q_1/p_1}\right) e_2 \\
\boldsymbol{u}_2 &= -\frac{p_1}{q_1}\boldsymbol{H}_0(\boldsymbol{q})\mathrm{diag}\left(\sigma_i^{-q_1/p_1}\right)\left(\gamma_\alpha \mathrm{sig}^{m_2/n_2}(\boldsymbol{s}) + \gamma_\beta \mathrm{sig}^{p_2/q_2}(\boldsymbol{s})\right) \\
\boldsymbol{s} &= \boldsymbol{e}_1 + \mathrm{sig}^{q1/p1}\left(\boldsymbol{\sigma}\boldsymbol{e}_2\right)
\end{aligned} \tag{46}$$

where $\boldsymbol{\Phi} = \mathrm{diag}\,(\Phi_1, \Phi_2, \ldots, \Phi_n)$ with $\Phi_i = -\alpha_{1i}\left(\frac{m_1}{n_1} - \frac{p_1}{q_1}\right) e_{1i}^{m_1/n_1 - p_1/q_1 - 1}\sigma_i^2 e_{2i}$, $\boldsymbol{\sigma} = diag\,(\sigma_1, \sigma_2, \ldots, \sigma_n)$ with $\sigma_i = \frac{1}{\alpha_1(i)e_{1i}^{m_1/n_1 - p_1/q_1} + \beta_1(i)}$, γ_α, γ_β, ζ are three positive constants, $\boldsymbol{\alpha}_1 = [\alpha_{11}, \alpha_{12}, \ldots, \alpha_{1n}]^{\mathrm{T}}$ and $\boldsymbol{\beta}_1 = [\beta_{11}, \beta_{12}, \ldots, \beta_{1n}]^{\mathrm{T}}$ with $\alpha_{1i} > 0$ and $\beta_{1i} > 0$, positive odd integers

https://doi.org/10.1017/aer.2024.128 Published online by Cambridge University Press

Table 2. *Parameters of the proposed controller*

Parameter	Values
Positive odd integer m_1	9
Positive odd integer n_1	7
Positive odd integer p_1	15
Positive odd integer q_1	17
Positive constant k_a	0.8
Positive constant k_b	0.6
Positive constant δ	0.001
Positive constant s_m	0.5
Positive constant s_n	0.5
Positive constant s_r	1
Positive odd integer m_2	9
Positive odd integer n_2	7
Positive odd integer p_2	15
Positive odd integer q_2	17
Control gain γ_1	0.8
Control gain γ_2	0.6
Control gain γ_3	0.4
Positive constant ss_m	0.5
Positive constant ss_n	1.2
Positive constant ss_r	2
Positive constant k_d	3
Positive constant l_k	0.5
Observation time T_d	0.5
Positive constant l_d	0.5
Positive constant δ_d	0.2
Control gain λ_{d1}	4
Control gain λ_{d2}	3
Initial state of $\mathbf{z}_d$	$[0.1, 0.15, -0.1, -0.15, 0.05, -0.05, 0.1]^{\mathrm{T}}$
Positive constant h_{1i}	5
Positive constant h_{2i}	6.4
Positive constant μ_i	1

$m_1, m_2, n_1, n_2, p_1, p_2, q_1, q_2$ satisfy the relationships $m_1/n_1 > 1, m_2/n_2 > 1, \frac{1}{2} < p_1/q_1 < 1, 0 < p_2/q_2 < 1$, and $m_1/n_1 - p_1/q_1 > 1$. To reduce the chattering phenomena, the saturation function is utilised in place of the function sgn $(\cdot)$ in the control design. The definition of the elements of sat $(\cdot)$ are

$$\mathrm{sat}(s_i) = \begin{cases} \mathrm{sgn}(s_i), & |s_i| \geq \varepsilon_0, \\ s_i/\varepsilon_0, & |s_i| < \varepsilon_0, \end{cases} \quad i = 1, 2, \ldots, 7 \tag{47}$$

with a positive small constant $\varepsilon_0 > 0$.

The ANFTSMC scheme is described as

$$\begin{aligned} \boldsymbol{u} &= \boldsymbol{u}_1 + \boldsymbol{u}_2 \\ \boldsymbol{u}_1 &= \boldsymbol{C}_0(\boldsymbol{q}, \dot{\boldsymbol{q}})\dot{\boldsymbol{q}} + \boldsymbol{H}_0(\boldsymbol{q})\ddot{\boldsymbol{q}}_d \\ &\quad - \boldsymbol{H}_0(\boldsymbol{q})\left(\alpha_1 \boldsymbol{K}_a \mathrm{diag}(|e_{1i}|^{\alpha_1 - 1})\boldsymbol{e}_2 + \boldsymbol{K}_b \dot{\boldsymbol{s}}_\rho\left(\boldsymbol{e}_1\right)\right) \\ \boldsymbol{u}_2 &= -\boldsymbol{H}_0(\boldsymbol{q})\left(\gamma_a \mathrm{sig}^{\alpha_2}(\boldsymbol{s}) + \gamma_b \mathrm{sig}^{p_2/q_2}(\boldsymbol{s})\right) - \boldsymbol{H}_0(\boldsymbol{q}) k\hat{\eta}\tanh(\boldsymbol{s}/\varepsilon) \\ \dot{\hat{\eta}} &= k\boldsymbol{s}^T \tanh(\boldsymbol{s}/\varepsilon) \\ \boldsymbol{s} &= \boldsymbol{e}_2 + \boldsymbol{K}_a \mathrm{sig}^{\alpha_1}\left(\boldsymbol{e}_1\right) + \boldsymbol{K}_b \boldsymbol{s}_\rho\left(\boldsymbol{e}_1\right) \end{aligned} \tag{48}$$

https://doi.org/10.1017/aer.2024.128 Published online by Cambridge University Press

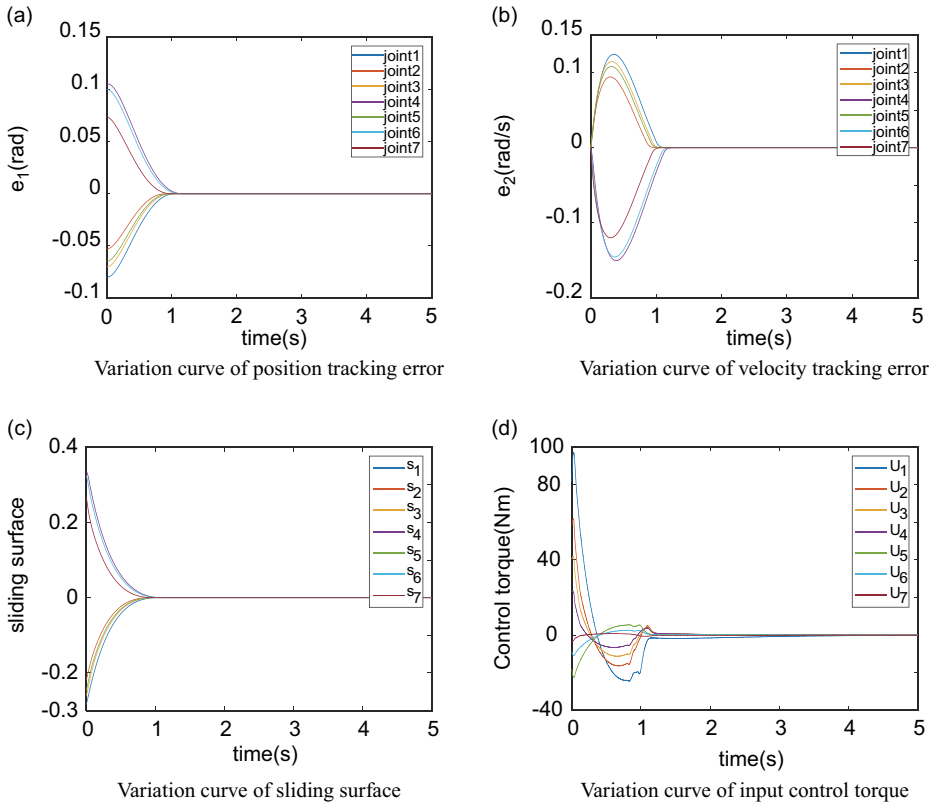


Figure 6. *Simulation results under DOBFTSMC.*

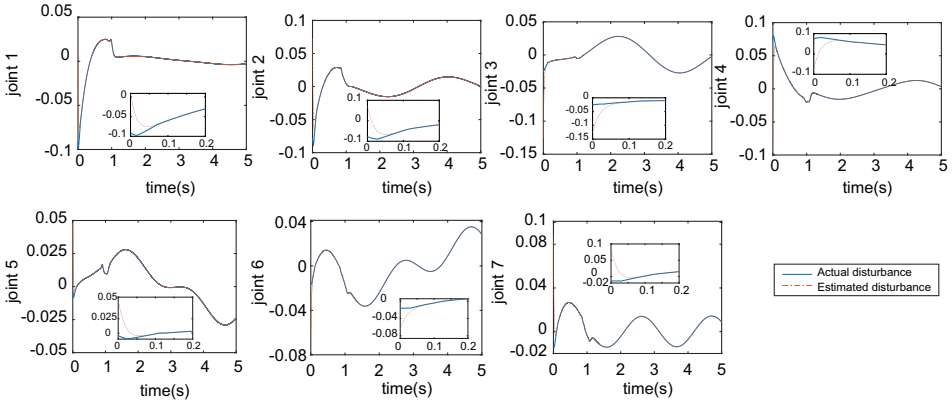


Figure 7. *Esitimation performance of lumped disturbance under DOBFTSMC.*

with the ith element of $\mathbf{s}_\rho$, which is expressed as

$$s_{\rho_i} = \begin{cases} \mathrm{sig}^{p_1/q_1}(e_{1i}), & \bar{s}_i = 0 \cup \bar{s} \neq 0, |e_{1i}| \geq \varepsilon_0 \\ l_1 e_{1i} + l_2 e_{1i}^2 \operatorname{sgn}(e_{1i}), & \bar{s} \neq 0, |e_{1i}| < \varepsilon_0 \end{cases} \tag{49}$$

where for a small positive constant ε_0, $l_1 = \left(2 - \frac{p_1}{q_1}\right) \varepsilon_0^{p_1/q_1 - 1}$, $l_2 = \left(\frac{p_1}{q_1} - 1\right) \varepsilon_0^{p_1/q_1 - 2}$, γ_a, γ_b, k are positive constants, $\boldsymbol{K}_a, \boldsymbol{K}_b$ are two positive definite matrices, $\alpha_1 = \frac{1}{2} + \frac{m_1}{2n_1} + \left(\frac{m_1}{2n_1} - \frac{1}{2}\right) \operatorname{sign}(||\mathbf{e}_1 - 1||)$,

https://doi.org/10.1017/aer.2024.128 Published online by Cambridge University Press

Table 3. *Control parameters for compared controllers*

Controllers	Parameters
FTSMC	$m_1 = 9, n_1 = 5, m_2 = 5, n_2 = 3, \gamma_\alpha = 2,$
	$p_1 = 7, q_1 = 9, p_2 = 5, q_2 = 9, \gamma_\beta = 2,$
	$\boldsymbol{\alpha}_1 = [1.5, 1.8, 1.5, 1.6, 1.8, 1.8, 1.2]$,
	$\boldsymbol{\beta}_1 = [0.8, 1.2, 1.2, 1.0, 0.8, 1.0, 1.2]$,
	$\zeta = 0.8, \varepsilon_0 = 0.01$
ANFTSMC	$m_1 = 9, m_2 = 9, n_1 = 7, n_2 = 7, \gamma_a = 0.8,$
	$p_1 = 11, p_2 = 9, q_1 = 13, q_2 = 13, k = 2.8,$
	$\boldsymbol{K}_a = \text{diag}\,(0.6, 0.8, 1.0, 0.8, 1.2, 0.8, 0.8)$,
	$\boldsymbol{K}_b = \text{diag}\,(0.8, 1.2, 1.2, 1.0, 0.8, 1.0, 1.0)$,
	$\gamma_b = 1.5, \varepsilon_0 = 0.001, \varepsilon = 0.01$

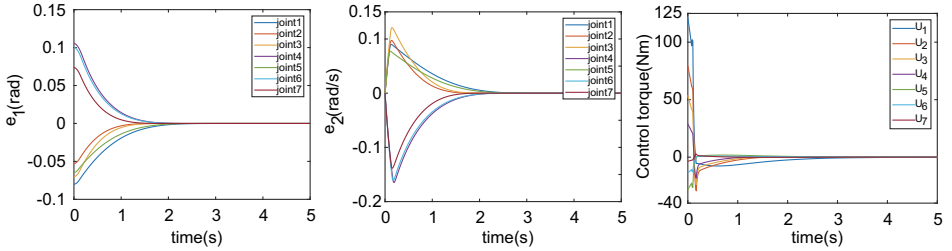


Figure 8. *Simulation results under FTSMC.*

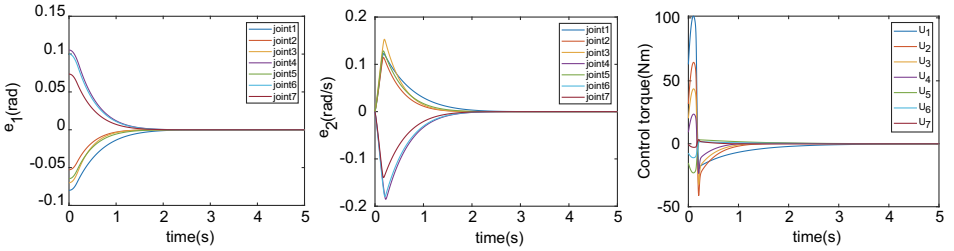


Figure 9. *Simulation results under ANFTSMC.*

$\alpha_2 = \frac{1}{2} + \frac{m_2}{2n_2} + \left(\frac{m_2}{2n_2} - \frac{1}{2}\right) \text{sign}\,(||\mathbf{s} - 1||)$, $\tanh\left(\frac{\mathbf{s}}{\varepsilon}\right) = [\tanh\left(\frac{s_1}{\varepsilon}\right), \tanh\left(\frac{s_2}{\varepsilon}\right), \ldots, \tanh\left(\frac{s_n}{\varepsilon}\right)]^{\mathrm{T}}$ with a constant $\varepsilon > 0$, $m_1, m_2, n_1, n_2, p_1, q_1$ are positive odd integers satisfying $m_1/n_1 > 1, m_2/n_2 > 1$ and $0 < p_2/q_2 < 1$.

For a fair and rational comparison, the simulations are conducted under the identical conditions. The selected control parameters for the two comparison controllers mentioned earlier are provided in Table 3. Figures 8 and 9 present the simulation results using FTSMC and ANFTSMC, respectively. In comparison with Fig. 6, all three controllers have finite convergence time, however, the suggested DOBFTSMC exhibits faster convergence. The norms of tracking position and velocity errors are shown in Fig. 10, demonstrating that the proposed controller has improved convergence and higher steady-state accuracy in more detail. Furthermore, three critical metrics – integrated absolute errors (IAEs), integrated time absolute errors (ITAEs), and energy consumptions (ECs) – are introduced to quantitatively evaluate the tracking performance of these controllers. Comparing the obtained indices displayed in Tables 4–6, it is observed that the suggested DOBFTSMC obtains the lower IAEs, ITAEs and ECs values than the other two referenced controllers. It is evident from this that the suggested controller outperforms the other two controllers with regard to tracking accuracy and convergence speed while consuming less energy.

https://doi.org/10.1017/aer.2024.128 Published online by Cambridge University Press

Table 4. *IAEs of the different controllers*

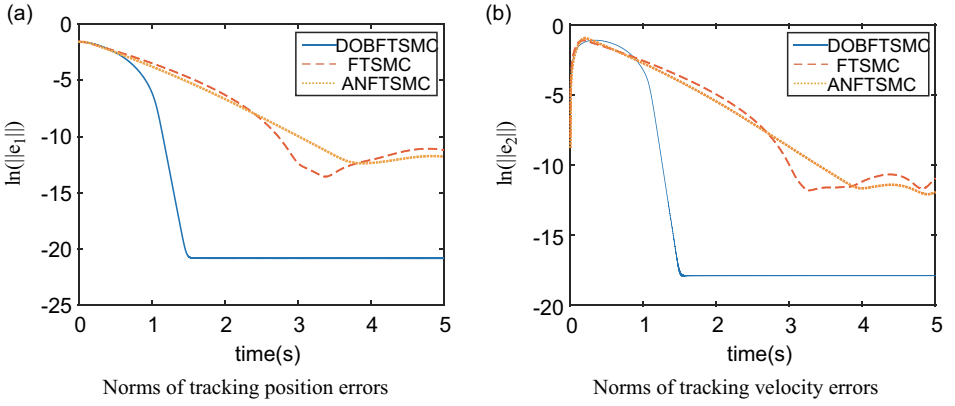
$IAE = \int_0^t \lvert e_{1i}(\varsigma)\rvert \, \mathrm{d}\varsigma$	DOBFTSMC	FTSMC	ANTSMC
IAE_{q_1}	0.1153	0.1351	0.1280
IAE_{q_2}	0.0730	0.0755	0.0754
IAE_{q_3}	0.0988	0.1023	0.0997
IAE_{q_4}	0.1556	0.1627	0.1606
IAE_{q_5}	0.0909	0.1063	0.0951
IAE_{q_6}	0.1469	0.1528	0.1513
IAE_{q_7}	0.1045	0.1059	0.1095

Table 5. *ITAEs of the different controllers*

$E_{q_i} = \int_0^t \varsigma \lvert e_{1i}(\varsigma)\rvert \, \mathrm{d}\varsigma$	DOBFTSMC	FTSMC	ANTSMC
$ITAE_{q_1}$	0.0099	0.0294	0.0229
$ITAE_{q_2}$	0.0049	0.0073	0.0073
$ITAE_{q_3}$	0.0075	0.0112	0.0094
$ITAE_{q_4}$	0.0152	0.0239	0.0219
$ITAE_{q_5}$	0.0068	0.0211	0.0113
$ITAE_{q_6}$	0.0139	0.0216	0.0202
$ITAE_{q_7}$	0.0082	0.0107	0.0136

Table 6. *ECs of the different controllers*

$EC_{ui} = \int_0^t \lvert u_i(\varsigma)\rvert^2 d\varsigma$	DOBFTSMC	FTSMC	ANTSMC
EC_{u_1}	1,283.6	1,311.5	1,511.0
EC_{u_2}	386.1	571.2	671.5
EC_{u_3}	170.0	269.4	317.1
C_{u_4}	47.9	86.4	102.6
EC_{u_5}	71.4	76.3	80.3
EC_{u_6}	16.3	18.1	18.7
EC_{u_7}	0.7	1.6	1.8



Norms of tracking position errors Norms of tracking velocity errors

Figure 10. *Norms of tracking position and velocity errors.*

https://doi.org/10.1017/aer.2024.128 Published online by Cambridge University Press

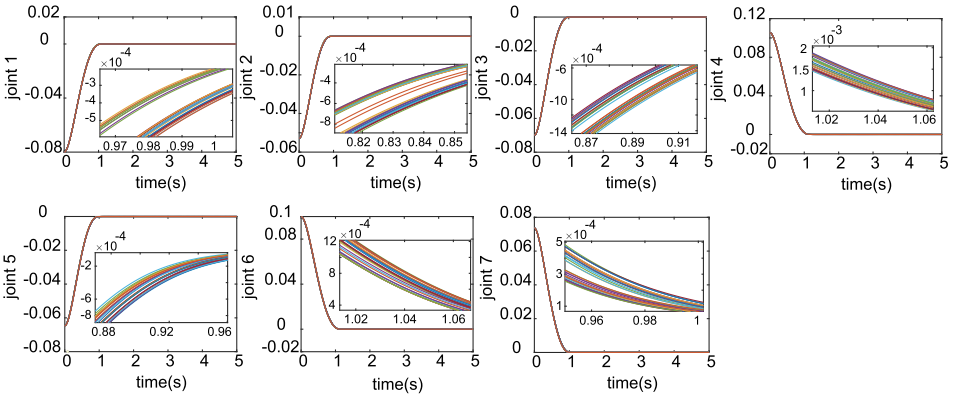


Figure 11. *Time response of the position tracking errors under the Monte Carlo tests.*

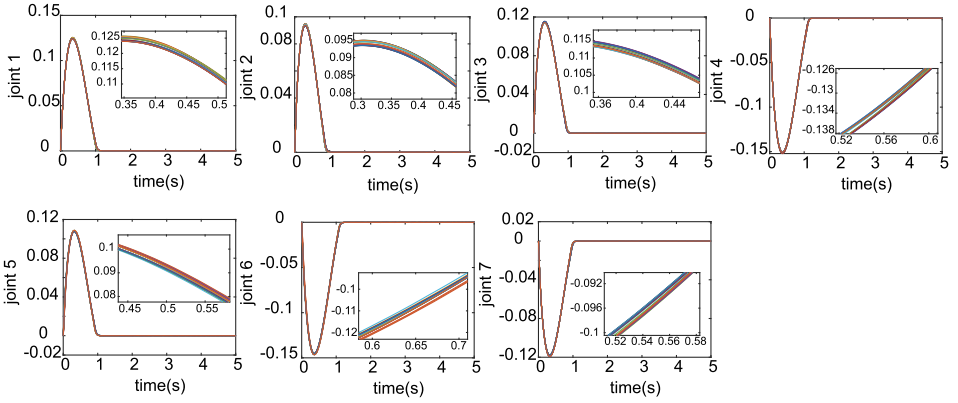


Figure 12. *Time response of the velocity tracking errors under the Monte Carlo tests.*

4.3 Monte Carlo tests

In this section, a total of 30 times Monte Carlo tests are executed to evaluate the robustness of the proposed DOBFTSMC method against parametric uncertainty and time-varying disturbance. Each trial subjects the space manipulator to a unique set of parametric uncertainties and time-varying disturbances. Specifically, the actual mass of each system component is set to $M_i' = M_i\,(1 + 0.1\mathcal{N}(0, 1))$, and the time-varying disturbances acting on the FFSM are chosen as $\boldsymbol{d}(t) = (2\mathcal{N}(0, 1) - 1)\,[0.03\cos(t), 0.01\cos(2t), 0.01\sin(2t), 0.03\sin(t), 0.02 + 0.01\varphi_d(t), 0.01\varphi_d(t), 0.01]^{\mathrm{T}}$ Nm, where $\varphi_d(t) = \sum_{r=0}^{N} b^{-rv_c}\sin(b^r t)$ is continuous but nowhere differentiable and limited, which attains continuous extended Caputo derivatives of any order $v < v_c$ [44]. Additionally, $\mathcal{N}(0, 1)$ is a randomised number following a standard Gaussian distribution. In the simulation, the values of $N = 200$, $b = 6$ and $v_c = 0.7$ are chosen. Besides, the remaining simulation conditions and the control parameter settings remain identical to those in Section 4.2.

The simulation results are illustrated in Figs 11–14. Figures 11 and 12 display the time responses of the position and velocity tracking errors under the Monte Carlo tests, respectively. Figure 13 shows the disturbance estimation of the proposed observer under the Monte Carlo tests. As evident from the figures, the change curves of position and velocity tracking errors under various test conditions are almost coincident. This suggests that the proposed controller effectively mitigates the adverse effects of parametric uncertainties and time-varying disturbances, thereby ensuring stable tracking performance within a fixed time. Figure 14 represents the time response of the control torques under the Monte Carlo

https://doi.org/10.1017/aer.2024.128 Published online by Cambridge University Press

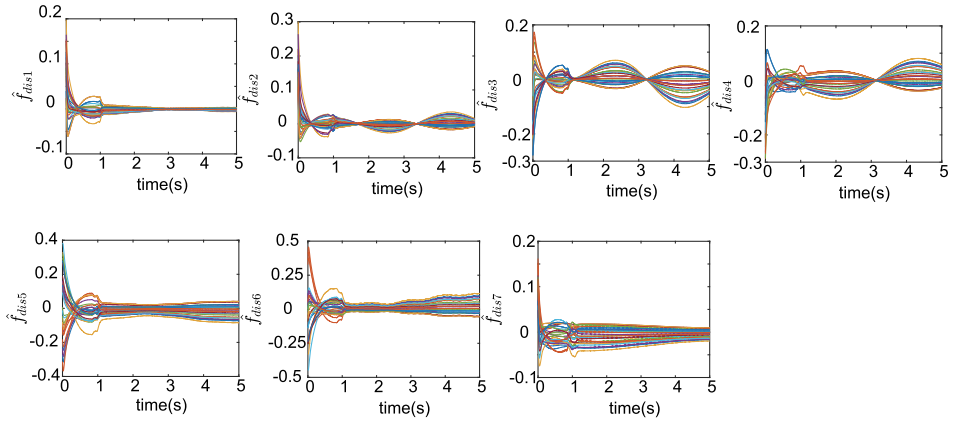


Figure 13. *The disturbance estimation of the proposed observer under the Monte Carlo tests.*

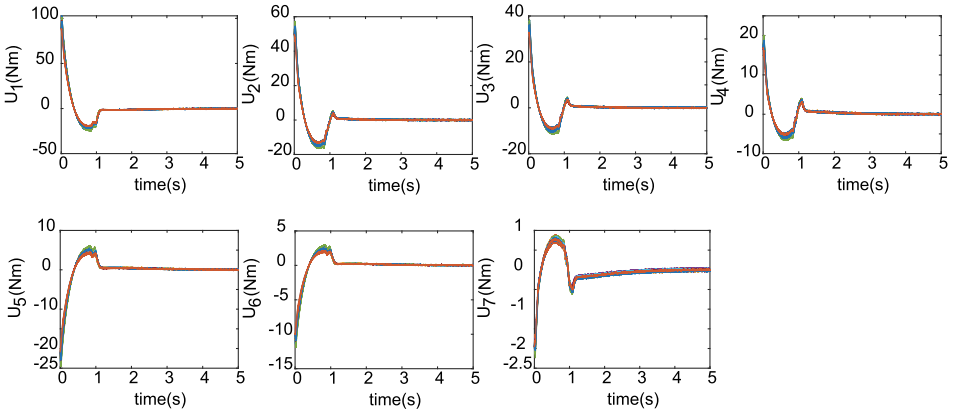


Figure 14. *Time response of control torques under the Monte Carlo tests.*

tests. Notably, at the beginning of the simulation, the control input is comparatively large, which is primarily attributed to a substantial initial tracking error coupled with an overestimation of the lumped disturbances. Based on the above analysis, it can be inferred that thanks to the excellent disturbance compensation capabilities of the observer, the proposed controller exhibits outstanding robustness against parametric uncertainties and time-varying disturbances. This guarantees the successful implementations of the specific on-orbit servicing missions, such as approaching or grasping a non-cooperative target.

Concluding from the aforementioned simulation results, the suggested DOBFTSMC scheme successfully solves the fixed-time trajectory tracking issue for space manipulator with parametric uncertainty and time-varying disturbance. Compared with the existing fixed-time control methods, the suggested method is verified to provide a better tracking performance when it comes to steady-state precision, convergence speed and control energy consumption.

5.0 Conclusion

In this paper, a new observer-based fixed-time sliding mode control approach was presented towards the trajectory tracking issue related to the space manipulator with parametric uncertainty and unknown disturbance. The proposed control strategy is based on the incorporation of a nonlinear disturbance observer

https://doi.org/10.1017/aer.2024.128 Published online by Cambridge University Press

in a faster fixed-time terminal sliding mode control. Despite the prior information of the lumped uncertainty remains unknown, the presented disturbance observer always enables accurate estimation and fast reconstruction of the lumped uncertainty within a specified time. Benefiting from such feed-forward compensation, the proposed controller assures that tracking errors of the position and the velocity converge to the origin within a fixed time, regardless of initial conditions. Simulation comparisons with existing fixed-time controllers demonstrate an excellent control performance of the suggested method in terms of faster convergence rate, higher tracking precision and less energy consumption. The primary focus of this paper is on the theoretical research of control algorithms. In the future, our work can primarily centre on two aspects. One is developing an experimental prototype to validate the performance of the devised controllers in real-world scenarios. Another is addressing more practical challenges encountered in controller development, such as actuator faults and time delays.

Competing interest. The authors declare that they have no conflict of known competing financial interests or personal relationships.

References

[1] Moosavian, S.A.A. and Papadopoulos, E., Free-flying robots in space: an overview of dynamics modeling, planning and control, *Robotica*, 2007, **25**, (5), pp 537–547.
[2] Flores-Abad, A., Ma, O., Pham, K. and Ulrich, S. A review of space robotics technologies for on-orbit servicing, *Progr. Aerospace Sci.*, 2014, **68**, pp 1–26.
[3] Shan, M., Guo, J. and Gill, E., Review and comparison of active space debris capturing and removal methods, *Progr. Aerospace Sci.*, 2016, **80**, pp 18–32.
[4] Li, W., Cheng, D., Liu, X., Wang, Y., Shi, W., Tang, Z., Gao, F., Zeng, F., Chai, H., Luo, W., Cong, Q. and Gao, Z. On-orbit service (oos) of spacecraft: A review of engineering developments, *Progr. Aerospace Sci.*, 2019, **108**, pp 32–120.
[5] Wang, H. and Xie, Y. Prediction error based adaptive jacobian tracking for free-floating space manipulators, *IEEE Trans. Aerospace Electron. Syst.*, 2012, **48**, (4), pp 3207–3221.
[6] Yang, H., Yu, Y., Yuan, Y. and Fan, X. Back-stepping control of two-link flexible manipulator based on an extended state observer, *Adv. Space Res.*, 2015, **56**, (10), pp 2312–2322.
[7] Kumar, N., Panwar, V., Borm, J.H., Chai, J. and Yoon, J. Adaptive neural controller for space robot system with an attitude controlled base, *Neural Comput. Appl.*, 2013, **23**, pp 2333–2340.
[8] Wang, M., Luo, J. and Walter, U., A non-linear model predictive controller with obstacle avoidance for a space robot, *Adv. Space Res.*, 2016, **57**, (8), pp 1737–1746.
[9] Rybus, T., Seweryn, K., and Sasiadek, J.Z. Control system for free-floating space manipulator based on nonlinear model predictive control (nmpc), *J. Intell. Rob. Syst.*, 2017, **85**, (3-4), pp 491–509.
[10] Zhang, F., Fu, Y. and Wang, S. An adaptive variable structure control of the robot satellite system with floating base in cartesian space, *Proc. Inst. Mech. Eng. Part C J. Mech. Eng. Sci.*, 2016, **230**, (18), pp 3241–3252.
[11] Xie, Z., Sun, T., Kwan, T. and Wu, X. Motion control of a space manipulator using fuzzy sliding mode control with reinforcement learning, *Acta Astronaut.*, 2020, **176**, pp 156–172.
[12] Seddaoui, A. and Saaj, C.M. Combined nonlinear h_∞ controller for a controlled-floating space robot, *J. Guid. Control Dyn.*, 2019, **42**, (8), pp 1878–1885.
[13] Guo, Y. and Chen, L. Terminal sliding mode control for coordinated motion of a space rigid manipulator with external disturbance, *Appl. Math. Mech.*, 2008, **29**, (5), pp 583–590.
[14] Shao, X., Sun, G., Xue, C., and Li, X., Nonsingular terminal sliding mode control for free-floating space manipulator with disturbance, *Acta Astronautica*, 2021, **181**, pp 396–404.
[15] Jia, S. and Shan, J., Finite-time trajectory tracking control of space manipulator under actuator saturation, *IEEE Trans. Ind. Electron.*, 2019, **67**, (3), pp 2086–2096.
[16] Jia, S. and Shan, J. Continuous integral sliding mode control for space manipulator with actuator uncertainties, *Aerospace Sci. Technol.*, 2020, **106**, p 106192.
[17] Yao, Q. Robust finite-time trajectory tracking control for a space manipulator with parametric uncertainties and external disturbances, *Proc. Inst. Mech. Eng. Part G J. Aerospace Eng.*, 2022, **236**, (2), pp 396–409.
[18] Polyakov, A., Efimov, D. and Perruquetti, W. Finite-time and fixed-time stabilization: Implicit lyapunov function approach, *Automatica*, 2015, **51**, pp 332–340.
[19] Jin, R., Rocco, P. and Geng, Y. Observer-based fixed-time tracking control for space robots in task space, *Acta Astronaut.*, 2021, **184**, pp 35–45.
[20] Yao, Q. Fixed-time neural adaptive fault-tolerant control for space manipulator under output constraints, *Acta Astronaut.*, 2023, **203**, pp 483–494.
[21] Cao, L., Xiao, B. and Golestani, M., Robust fixed-time attitude stabilization control of flexible spacecraft with actuator uncertainty, *Nonlinear Dyn.*, 2020, **100**, pp 2505–2519.

https://doi.org/10.1017/aer.2024.128 Published online by Cambridge University Press

[22] Pan, H., Zhang, G., Ouyang, H. and Mei, L. Novel fixed-time nonsingular fast terminal sliding mode control for second-order uncertain systems based on adaptive disturbance observer, *IEEE Access*, 2020, **8**, pp 126615–126627.
[23] Liu, Y., Yan, W., Zhang, T., Yu, C. and Tu, H. Trajectory tracking for a dual-arm free-floating space robot with a class of general nonsingular predefined-time terminal sliding mode, *IEEE Trans. Syst. Man Cybern. Syst.*, 2021, **99**, pp 1–14.
[24] Wan, L., Cao, Y., Sun, Y., and Qin, H. Fault-tolerant trajectory tracking control for unmanned surface vehicle with actuator faults based on a fast fixed-time system, *ISA transactions*, 2022, **130**, pp 79–91.
[25] Wu, C., Yan, J., Wu, X., Guo, Y., Mou, P. and Xiao, B., Predefined-time sliding manifold-based fixed-time attitude stabilization control of receiver aircraft with measurement noises, *Trans. Inst. Meas. Control*, 2022, **44**, (11), pp 2193–2203.
[26] Jin, M., Kang, S.H. and Chang, P.H. Robust compliant motion control of robot with nonlinear friction using time-delay estimation, *IEEE Trans. Ind. Electron.*, 2008, **55**, (1), pp 258–269.
[27] Roy, S. and Kar, I. Adaptive sliding mode control of a class of nonlinear systems with artificial delay, *J. Franklin Inst.*, **10** 2017, 354, pp 8156–8179.
[28] Chen, W., Ballance, D.J., Gawthrop, P.J. and O'Reilly, J. A nonlinear disturbance observer for robotic manipulators, *IEEE Trans. Ind. Electron.*, 2000, **47**, (4), pp 932–938.
[29] Hu, Q., Li, B. and Qi, J. Disturbance observer based finite-time attitude control for rigid spacecraft under input saturation, *Aerospace Sci. Technol.*, 2014, **39**, pp 13–21.
[30] Yu, X. and Chen, L. Observer-based two-time scale robust control of free-flying flexible-joint space manipulators with external disturbances, *Robotica*, 2017, **35**, (11), pp 2201–2217.
[31] Zhu, Y., Qiao, J. and Guo, L., Adaptive sliding mode disturbance observer-based composite control with prescribed performance of space manipulators for target capturing, *IEEE Trans. Ind. Electron.*, 2019, **66**, (3), pp 1973–1983.
[32] Yao, Q. Disturbance observer-based robust fixed-time integrated trajectory tracking control for space manipulator, *Robotica*, 2022, **40**, (9), pp 3214–3232.
[33] Zuo, Z. Non-singular fixed-time terminal sliding mode control of non-linear systems, *IET Control Theory Appl.*, 2015, **9**, (4), pp 545–552.
[34] Zhang, Y., Tang, S. and Guo, J. Adaptive terminal angle constraint interception against maneuvering targets with fast fixed-time convergence, *Int. J. Robust Nonlinear Control*, 2018, **28**, pp 2996–3014.
[35] Polyakov, A. Nonlinear feedback design for fixed-time stabilization of linear control systems, *IEEE Trans. Autom. Control*, 2011, **57**, (8), pp 2106–2110.
[36] Jiang, B., Hu, Q. and Friswell, M.I. Fixed-time attitude control for rigid spacecraft with actuator saturation and faults, *IEEE Trans. Control Syst. Technol.*, 2016, **24**, (5), pp 1892–1898.
[37] Cao, L., Xiao, B., Golestani, M. and Ran, D., Faster fixed-time control of flexible spacecraft attitude stabilization, *IEEE Trans. Ind. Inf.*, 2019, **16**, (2), pp 1281–1290.
[38] Ni, J., Liu, L., Liu, C., Hu, X. and Li, S. Fast fixed-time nonsingular terminal sliding mode control and its application to chaos suppression in power system, *IEEE Trans. Circ. Syst. II Exp. Briefs*, 2017, **64**, (2), pp 151–155.
[39] Liu, Y., Wang, H. and Fan, J. Novel docking controller for autonomous aerial refueling with probe direct control and learning-based preview method, *Aerospace Sci. Technol.*, 2019, **94**, p 105403.
[40] Su, Z., Wang, H., Yao, P., Huang, Y. and Qin, Y. Back-stepping based anti-disturbance flight controller with preview methodology for autonomous aerial refueling, *Aerospace Sci. Technol.*, 2017, **61**, pp 95–108.
[41] Li, H. and Cai, Y. Fixed-time non-singular terminal sliding mode control with globally fast convergence, *IET Control Theory Appl.*, 2022, **16**, (12), pp 1227–1241.
[42] Cruz-Zavala, E., Moreno, J.A. and Fridman, L.M. Uniform robust exact differentiator, *IEEE Trans. Autom. Control*, 2011, **56**, (11), pp 2727–2733.
[43] Yan, Y., Cui, H. and Han, P. Fixed-time control for free-floating space manipulators with prescribed constraints and input saturation, *Aeronaut. J.*, 2023, **128**, (1324), pp 1–26.
[44] Dou, B. and Yue, X. Disturbance observer-based fractional-order sliding mode control for free-floating space manipulator with disturbance, *Aerospace Sci. Technol.*, 2023, **132**, p 108061.

Cite this article: Yan Y.X., Cui H. and Han P. (2025). Disturbance observer-based fixed-time tracking control for space manipulators with parametric uncertainty and unknown disturbance. *The Aeronautical Journal*, **129**, 1399–1420. https://doi.org/10.1017/aer.2024.128

https://doi.org/10.1017/aer.2024.128 Published online by Cambridge University Press